Sedimentologika

Research article

# From flood to turbidity current: combined models to simulate continent to ocean sediment transport in the Var system, France

Arthur Remaud[1], John J. Armitage[1*], Vanessa Teles[1], Sébastien Rohais[1], Thierry Mulder[2]

[1] Direction Sciences de la Terre et Technologies de l'Environnement, IFP Energies nouvelles, France
[2] Université de Bordeaux, CNRS UMR5805 EPOC, France

*corresponding author: John J. Armitage (john-joseph.armitage@ifpen.fr)

doi: 10.57035/journals/sdk.2024.e22.1538

Editor: Ian Kane
Reviewers: Elda Miramontes and one anonymous reviewer
Copyediting, layout and production: Romain Vaucher, Georgina Virgo and Sophie Hage

Submitted: 22.05.2024
Accepted: 30.07.2024
Published: 02.09.2024

**Abstract |** Turbidity currents are a form of gravity-driven flow that occurs in subaqueous environments. These currents contain a low volumetric percentage of particles but are very important in transporting them from coastal to deep-marine environments. In the Var sediment routing system, southeastern France, there is a sedimentary record of turbidity currents formed by submarine landslides and flooding of the Var River. In 2006, there was continuous monitoring of the marine section that recorded four turbidity currents. To explore the connectivity between the terrestrial source and marine basin we linked two reduced complexity models of sediment transport and landscape change. The aim of the paper is to combine two models, one dedicated to the prediction of river water and sediment run-off, and the second dedicated to the transport, erosion, and sedimentation by a turbidity current. The landscape evolution model CAESAR-Lisflood was used to model discharge and sediment yield. The behaviour of turbidity currents was modelled with the cellular automata model CATS. From calibration of the two models against observations of discharge and suspended sediment in the Var River system, we find that in 2006, two rainfall events would have led to hyperpycnal turbidity currents. These two events match well with two of the four-recorded events. Focusing on the largest event we find that the source pulse of sediment from the terrestrial environment is short-lived, less than half a day, but contains a significant quantity of fine particles. The event transferred on the order of $10^5$ $m^3$ of suspended sediment from source to sink. This study demonstrates that hyperpycnal turbidity currents can be generated with concentrations as low as 2-6 $kg/m^3$ at the Var River mouth far below the theoretical 40 $kg/m^3$ threshold, suggesting active convective sedimentation in the surface plume and sea-water dilution at the flooding river mouth. A substantial amount of sediment (35% of the input volume) is directly transferred towards the deepest part of the system during a short-living hyperpycnal turbidity current. However, a considerable (65%) part remains in the surface as a hypopycnal plume feeding the hemipelagic sedimentation.

**Lay summary |** Turbidity currents are gravity-driven flows of suspended sedimentary material within the water column. They occur in the marine environment where the sea floor drops steeply from the coastline into the deep sea and can be triggered by slope failure and sediment released into the marine environment from river systems. The Var submarine canyon system has a geological and recent record of turbidity currents caused by sediment discharge from the upstream Var River catchment. Here we explore the connectivity between the river and the marine systems with two numerical models, each dedicated to both ends of the continuum from the continental to the marine domain. Our models imply a strong relationship between river flooding and turbidity currents, however less than half of the sediment discharged by the river system is transported by the turbidity current. This implies that a significant quantity of terrestrial particulate material remains in the surface marine environment post-flooding, with implications for the wider and non-local dispersion of both sediments and particulate pollution from river systems.

**Keywords**: Hyperpycnal flows, Source-to-sink, Sediment discharge, Turbidity current, Reduced complexity numerical modelling

## 1. Introduction

The Var catchment is a classic steep sloped Mediterranean catchment that is known to generate significant flood-related runoff events that are related to landslides and associated with large quantities of sediment release (Anthony & Julian, 1999). It is the largest catchment in the French Riviera, with a watershed of 2820 km$^2$, and a significant range in topography from the coast to high altitude summits of the Alpine Mercantour massif at 3143 m (Figure 1). Flash floods are recorded in the marine sediment as turbidite deposits related to hyperpycnal flows (Mulder et al., 1998). In the last two decades, more than 12 storms have caused significant flooding along the Mediterranean coastline, and the cost of the damage is often greater than 1 billion euros for each event (Gourbesville & Ghulami, 2022). The most recent was Storm Alex in October 2020. It caused intense precipitation in the interior of the Alps-Maritimes and the northeast of the Var with more than 330 mm rainfall over the whole watershed within 24 h (Gourbesville & Ghulami, 2022). Satellite images of the outlet of the Var after the storm showed a large surface (hypopycnal) plume carrying fine particles heading into the Mediterranean (Figure 1). Meanwhile, within the catchment, ten people died and hundreds of houses and infrastructure such as a hydropower plant, wastewater treatment plants, up to 200 km of roads, and six bridges were destroyed. Furthermore, the Vésubie tributary to the Var, along with the Roya catchment that is next to the Var, saw significant channel widening and sediment transport during and post-storm (Liébault et al., 2024), which would imply that the destruction was likely caused by both the rapidly flowing water and the significant quantities of sediment brought with the flowing water.

Sedimentary deposits within the marine end of the Var source-to-sink system likely record past flood events, as the suspended sediment load plunges into the deep marine system and becomes a turbidity current (Gennesseaux, 1962; Mulder et al., 1998). Therefore, the marine record could provide information on the past frequency of such powerful storm events and help understand how the landscape might respond to future increases in such storms. The complication is that hyperpycnal flows are not the only process that can generate turbidity currents and their related sedimentary deposits in this submarine depositional system. Turbidity currents are also frequently generated from slope failures within the shallow marine regions of the canyon systems due to overloading, oversteepening, and potentially regional earthquakes (Mulder et al., 1994; Piper & Savoye, 1993). In 1979, a submarine slump was also initiated, from a singular triggering event, during the civil engineering work for the extension of the yacht harbour just next to Nice airport (Habib, 1994), and transformed into a turbidity current that deposited an up to 1 m thick turbidite in some parts the submarine canyon (Gennesseaux et al., 1980; Piper & Savoye, 1993; Mulder et al., 1998).

Between 2005 and 2007, there was continuous monitoring of the Var Canyon system (Khripounoff et al., 2009; Mas, 2009). These observations give an extensive set of data that can be used to test models of the relationship between the rainfall input at the source and the observed sedimentary response at the sink. Numerical modelling of the source-to-sink system has received some attention for long-timescale processes at the basin scale (e.g., Ding et al., 2019). However, to our knowledge there are very few studies for short-timescale events. One challenge is the complexity of the hydrological and sedimentological processes. For example, the rainfall to runoff and river flow involves multiple processes at different scales from infiltration to the propagation of a flood wave down the system. Turbidity currents are likewise complex physical phenomena, generated from the turbulent flow of mixtures of sediment and water down marine slopes interacting along the way with the sea floor (e.g., Talling et al., 2023). In addition, turbidity currents are usually bipartite with a basal concentrated laminar flow capped with a thick turbulent upper part (Postma et al., 1988). Reduced complexity models that try to find the compromise between simple laws to capture the first-order observations, can help in understanding the link between floods and turbidity flows. Following that line of thought, in this article, we will explore if two reduced-complexity models, CAESAR-Lisflood (Coulthard et al., 2013) and CATS (Teles et al., 2016) can capture the system response. We will constrain what range of values are suitable for the two models to match the observed durations and magnitudes of continental flood and turbidity current events. In addition, we will investigate if such reduced-complexity models can be useful for predicting the connectivity of source-to-sink systems for flood-related pollution and sediment transport.

## 2. The Var source-to-sink system - Observations and Data

The upper Var watershed (Figure 1) is characterised by a marked topography and low vegetation cover, resulting in high denudation rates (catchment average of 0.24±0.04 mm/yr.; Mariotti et al., 2019). The steep slopes (maximum of 86° and mean of 25° calculated from a 5 x 5 m resolution digital elevation model (DEM); Ma & Gourbesville, 2020) give the river system a torrential character and short reaction times. The cut over the Callovian-Oxfordian "Terres Noires" (black shales) can provide easily erodible material during strong rainfalls, forming usually subaerial debris flows (Grandjean et al., 2006). The average slope of the downstream reach is much less pronounced with a braided pattern composed of coarse alluvium (Chapuis et al., 2018).

The turbidite system of the Var is sand-rich and located in the Ligurian Sea (southeastern France). The continental shelf off Nice is almost absent or very narrow (2–3 km) with a steep continental slope of between 6° and 15°. The result is that the Var Canyon connects to the mouth of the

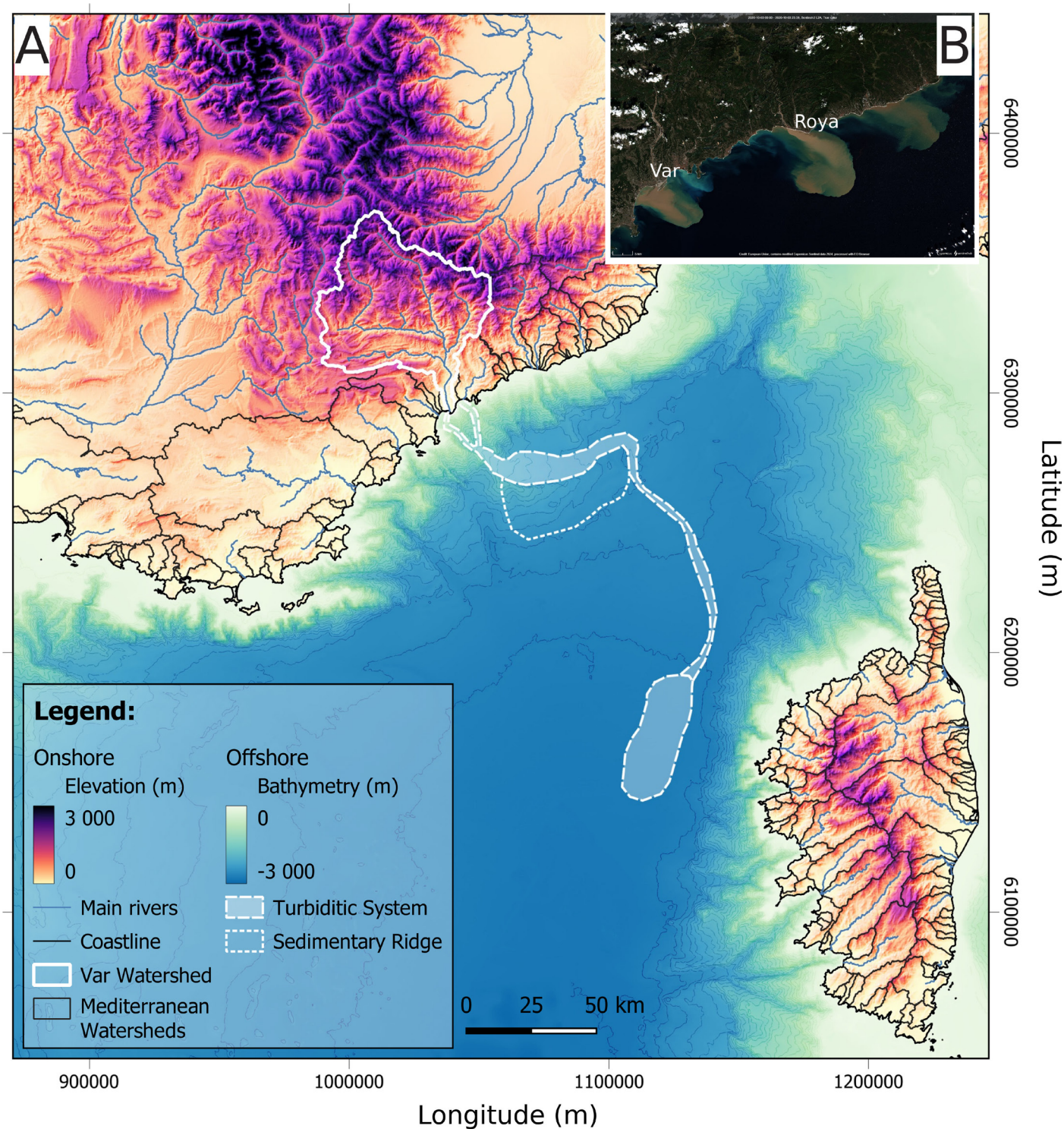


**Figure 1 |** (A) Location map of the Var source-to-sink system. The source is the Var watershed, and the sink is the turbidite system that passes through two canyons with an area of deposition around the sedimentary ridge and at the end of the canyon system. (B) Inset on the top right is a Sentinel II satellite image from the 3rd of October 2020 showing the hypopycnal plumes that carried sediment out of the Var and Roya rivers (Copernicus Sentinel data 2020). Bathymetry is from EMODnet with contours at 100 m intervals within the deeper marine setting, and the projection is Lambert93.

Var River (Figure 1). The submarine turbidite system of the present Var is estimated to have a total surface area of 16,320 km² (Migeon et al., 2000) and a length of 250 km from the mouth of the Var to its outermost part of the terminal fan, offshore eastern Corsica Island (Figure 1). Following the Canyon, a large valley (called the Var Valley) opens with three different channel routes bordered by a hypertrophied right-handed levee called the Var Sedimentary Ridge (Piper & Savoye, 1993).

Three types of initiation mechanisms have been recognized for sediment transport in the Var slope submarine system (Mulder et al., 1998): large, probably earthquake-induced, turbidity currents (Mulder et al., 1994); small-sized, failure-related low-density turbidity currents (Gennesseaux, 1962; Gennesseaux et al., 1971) and hyperpycnal flows related to large floods (Mulder et al., 2001). Related turbidites are deposited in the Var Valley such as for the 1979 turbidity current (Gennesseaux et al., 1980;

Piper & Savoye, 1993) but also by overspill on the Var levee (Migeon et al., 2001).

### 2.1. Topographic data

The digital elevation model (DEM) for the Var catchment was generated from a merging of the Alpes-Maritimes DEM (27/04/2018) and the Alpes-de-Haute-Provence DEM (05/05/2020) derived from satellite and Lidar data (acquired in possible flood zones) with a resolution of 25 x 25 m. It was downloaded from the BD ALTI® catalogue on the IGN website at the following address: https://geo-services.ign.fr/bdalti. The bathymetry map comes from the three research cruises that were part of the MELISAR project running from 2006 to 2008 along the Ligurian margin using the R/V Le Surtôt (Migeon et al., 2011; Migeon, 2006; Figure 2). The bathymetry dataset is of a resolution of 25 x 25 m and was lowered to 200 x 200 m to be able to represent the geometry of the C2 Terrace where the core MTB-VA-26 is situated and still has reasonable model run times (Figure 2).

### 2.2. Hydrological data

For the Var source-to-sink system, offshore turbidity current measurements are available for the periods from August 1st, 2006, to December 30th, 2006 (Khripounoff et al., 2009; Mas, 2009). We therefore searched for available high-resolution precipitation data and river discharge measurements that correspond with the same time window.

#### 2.2.1. Precipitation data

The meteorological data come from the Publithèque of Météo France (https://publitheque.meteo.fr/). For autumn and winter 2006, there are different types of rainfall distributions: August rainfalls are distributed across almost the whole watershed, with a slight clustering towards the eastern Alpine side of the catchment. Subsequently, there is a period of a few days with large amounts of rainfall across the catchment. A large rainfall event was recorded at the northern station of Peone in early September, which was followed by more distributed rainfall and a significant rainfall event around the 25th of September. In late November and early December, rainfall occurs mostly around Nice, while in December, there is precipitation across the whole catchment. Data from 14 active hourly rainfall stations in 2006 within and near the watershed were used to create spatially variable input rainfall for CAESAR-Lisflood (Figure 3). Rainfall stations were interpolated onto the catchment DEM using the nearest neighbour algorithm from the SciPy Python library (Virtanen et al., 2020) (Figure 3A). This simple method allows the spatial distribution of rainfall events to be input into the model.

#### 2.2.2. Discharge measurements

Discharge measurements recorded since 1974 are available on the SCHAPI HydroPortail website at the following address: https://www.hydro.eaufrance.fr/. They can be in the form of daily average or instantaneous discharges every 3 h. The discharge measurement station located furthest downstream in the system is at the Napoléon III Bridge, which is ~1 km from the mouth of the Var River (Nice, Figure 1). It records all the flood events that may have generated a turbidity flow in the Mediterranean Sea (Mas, 2009).

#### 2.2.3. Turbidity currents data

Offshore measurements for a combined period of 20 months from October 2005 to May 2007 are described in Khripounoff et al. (2009) and Mas (2009). During this period, five moorings with sediment traps and current meters were deployed on each station along the axis of the Var Canyon at water depths ranging from 1200 m to 2300 m. Two of these moorings picked up turbidity currents from autumn to winter 2006 (Figure 2; Table 1). The moorings also had a current meter recording the speed, direction, temperature, and pressure of the current every 30 minutes.

The 25th September 2006 event, coinciding with the flood of the Var River, is recorded from 18h00 at mooring VV for a

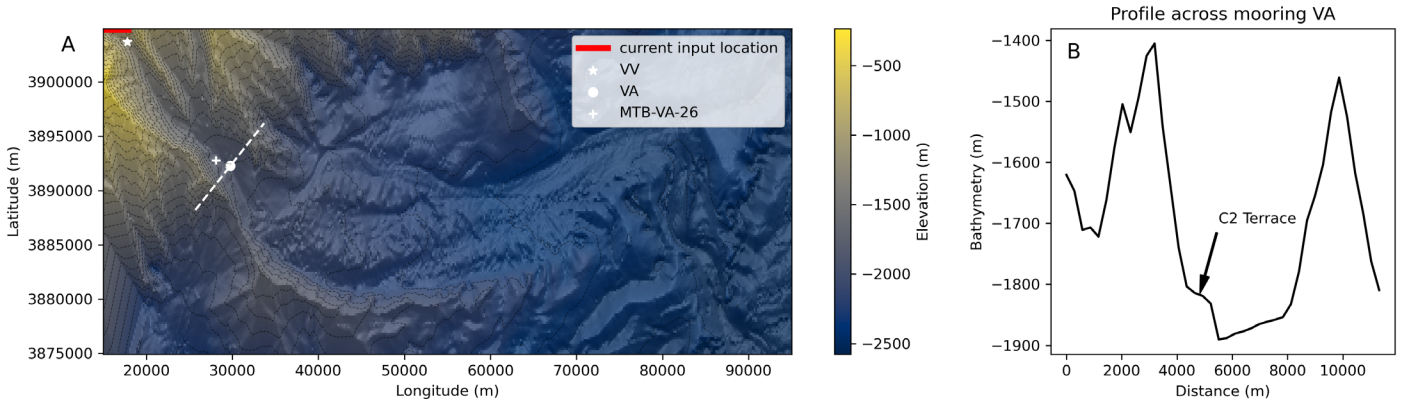


**Figure 2 |** Bathymetry of the Var Canyon with the zone of turbidity current initiation shown in red at the top left corner of the basin. (A) Bathymetric map of the upper Var Canyon showing the location of the sediment traps at points VV and VA and the location of the core at location MTB-VA-26. (B) Cross section centred on the point VA as displayed by the dashed line in (A). The C2 terrace can be seen just right of centre. Data is from Migeon (2006). The projection is Lambert93.

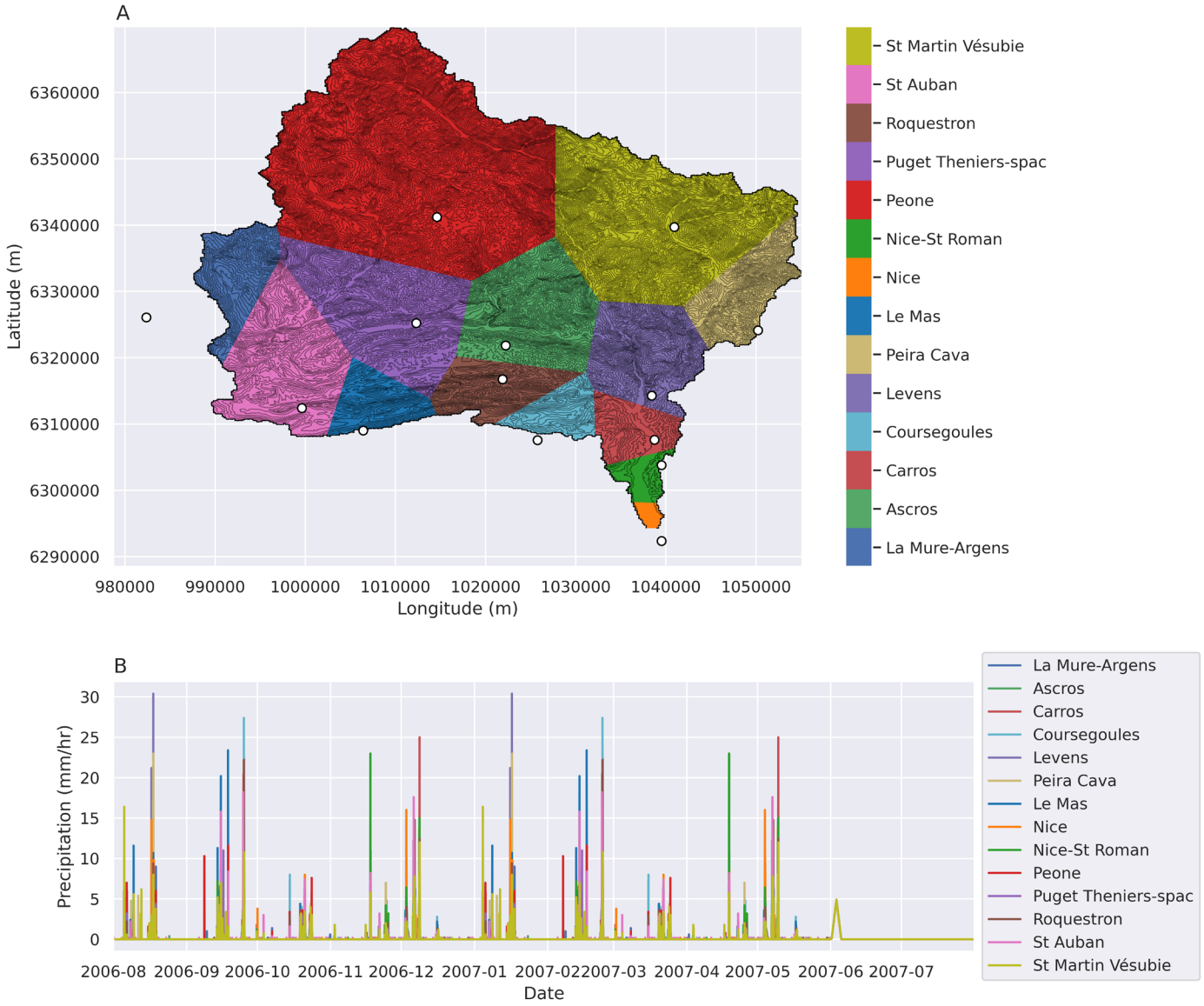


**Figure 3 |** Rainfall weather station coverage and time series. (A) Map of the rainfall polygons for the 14 weather stations that provide hourly rainfall for 2006. The polygons are centred on the rainfall stations (circle markers) using the nearest neighbour algorithm from the SciPy Python library (Virtanen et al., 2020). The projection is Lambert93. (B) Precipitation between August and December 2006 for the 14 weather stations.

| Name | Start date | End date | Location | Depth | Content | Position above seafloor |
|---|---|---|---|---|---|---|
| VV | 26/09/2005 | 08/10/2007 | Var Canyon | 1200 m | Particle trap<br>Current meter | 20 m<br>30 m |
| VA | 25/09/2005 | 08/10/2007 | Upper Valley | 1850 m | Particle trap<br>Current meter<br>Particle trap<br>Current meter | 20 m<br>30 m<br>450 m<br>460 m |

**Table 1 |** Data on the marine mooring and sediment traps whose locations are available in Figure 2 (from Mas, 2009).

total duration of 27 h (Figure 4). Concerning the velocities recorded at 30 m of height, a sharp increase is recorded up to 0.47 m/s at 18h30, followed by a serrated evolution, with a maximum peak value of 0.57 m/s at 23h00. The temperature evolution, also uneven, shows a progressive increase from a value of 13.15°C to a maximum value of 13.5°C (Figure 4) suggesting warmer continental water input. The same event is also observed roughly 15 km downstream at the mooring VA starting September 26$^{th}$ at 6h00 and lasting 7h30 (Figure 4). The delay between the record of this turbidity current at each station is 12 h.

## 2.3. Sedimentary data

### 2.3.1. Continental system

There is very little information on the grain size distribution of the sediments entering the Var system. Within the

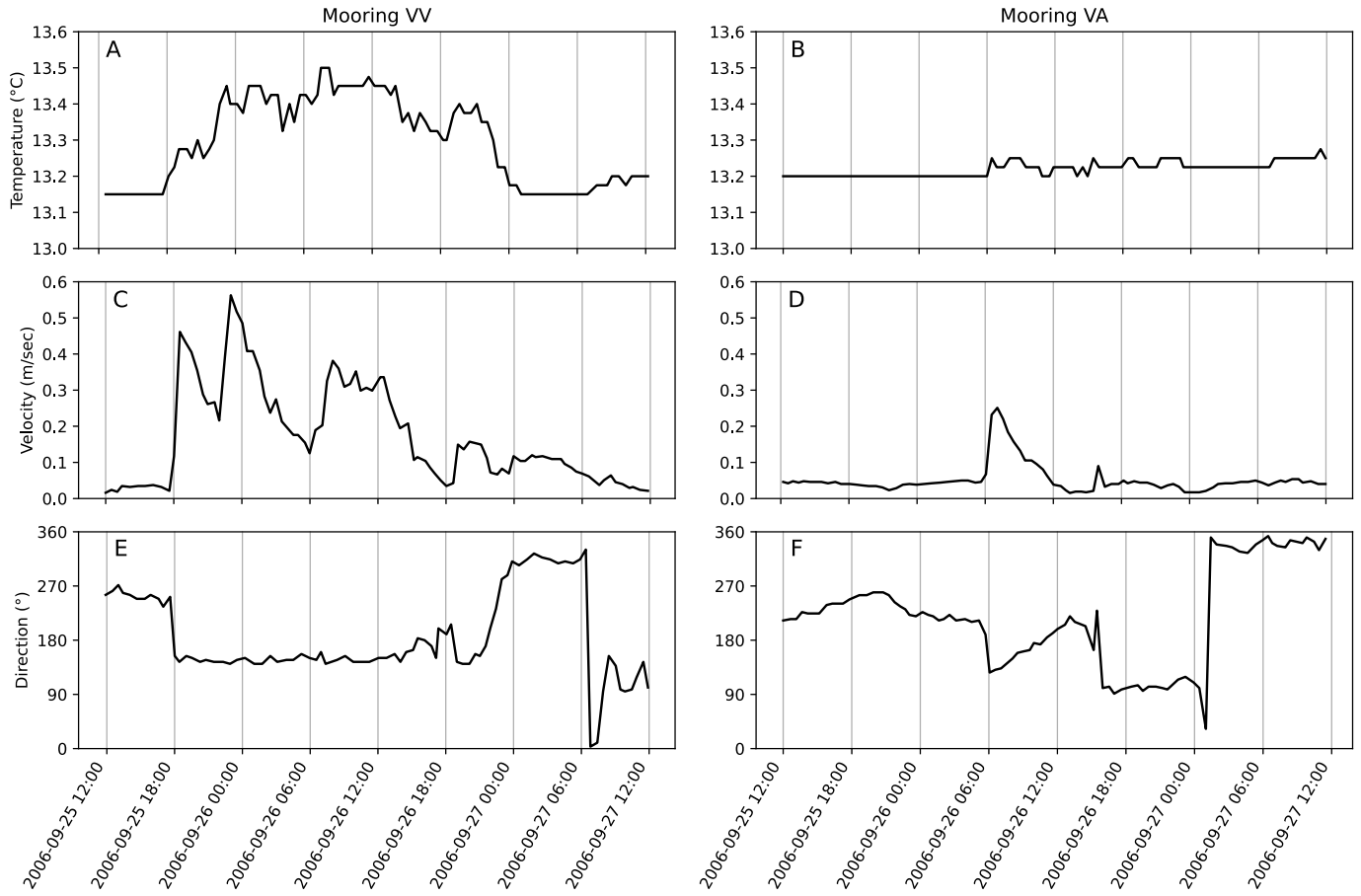


**Figure 4 |** Water properties at moorings VV and VA in the Var Canyon system. (A, B) temperature (°C), (C, D) flow velocity (m/sec), (E, F) flow direction (0° is magnetic north) of the currents during the 25th September 2006 event (observations digitized from Mas, 2009).

"grey literature" (technical reports from the BRGM and the Syndicat Mixte d'Etudes de la Basse Vallée du Var) there is some information on the gravel grain size and sediment discharge. Measurements from various gravel bars within the alluvial plain suggest a mean grain size between 3 and 5 cm (Pebbles; Jaeggi, 2003). From these estimates and the annual discharge, the bedload is estimated to be 31,000 $m^3$/yr (Jaeggi, 2003). This estimate is significantly lower than reported by the BRGM, with bedload discharge estimated to be greater than 100,000 $m^3$/yr (Oliveros, 1996). The discrepancy is likely due to the improvement of methods for estimating the bed slope within the catchment. Annual suspended loads are estimated to be between $1\times10^6$ and $6\times10^6$ $m^3$/yr (Laurent, 1971; Oliveros, 1996).However these might likewise be an overestimation following the same arguments used for bed load estimates. Note that the bedload transport has been drastically reduced since damming during the last century of the lower watershed and the reclamation of land within the lower valley and delta (Anthony, 1995).

In the absence of observations of the fine grains, the proportion of sediment grain sizes is estimated from the SoilGrids map of the region (Poggio et al., 2021). The map is interpolated from a large database of soil measurements to a resolution of 250 x 250 m (Poggio et al., 2021). Based on the relative proportion of clay, silt, sand, and coarse material (gravel) within the top 30 cm from the SoilGrids dataset, we can estimate the fraction of each grain size for the model catchment. (Table 2). We generate three grain size classes by combining the clay and silt classes and giving this combined group the characteristic grain size of silt (Table 2). For gravel we assume a mean grain size of 2 cm. We take this slightly smaller grain size for the gravel source compared to that observed within the alluvial cover to be consistent with the SoilGrids dataset. These three grain sizes are then transported down-system, with the combined silt and clay forming the suspended load, and the sand and gravel forming the bedload.

| **Classification** | Clay & Silts | Sand | Gravels |
|---|---|---|---|
| **Grain size** | 32 µm | 0.5 mm | 2 cm |
| **Proportion** | 57% | 26% | 17% |

**Table 2 |** Depth-weighted averages (top 30 cm) of the proportions of each grain type in the Var catchment.

### 2.3.2. Marine turbidite deposits

As part of the ENVAR-HERMES marine campaigns (e.g., Khripounoff et al., 2009), interface cores were sampled every 6 months between September 2005 and August 2007 on the different morphological units of the system (terraces, channel, Var sedimentary ridge) to quantify the sediments deposited during the time of deployment of the moorings. Analysis of these new sedimentary deposits allowed Mas (2009) to identify three new sequences deposited between September 2006 and April 2007 on sub-terrace C2 (MTB-VA-26, Figure 5). These sequences all

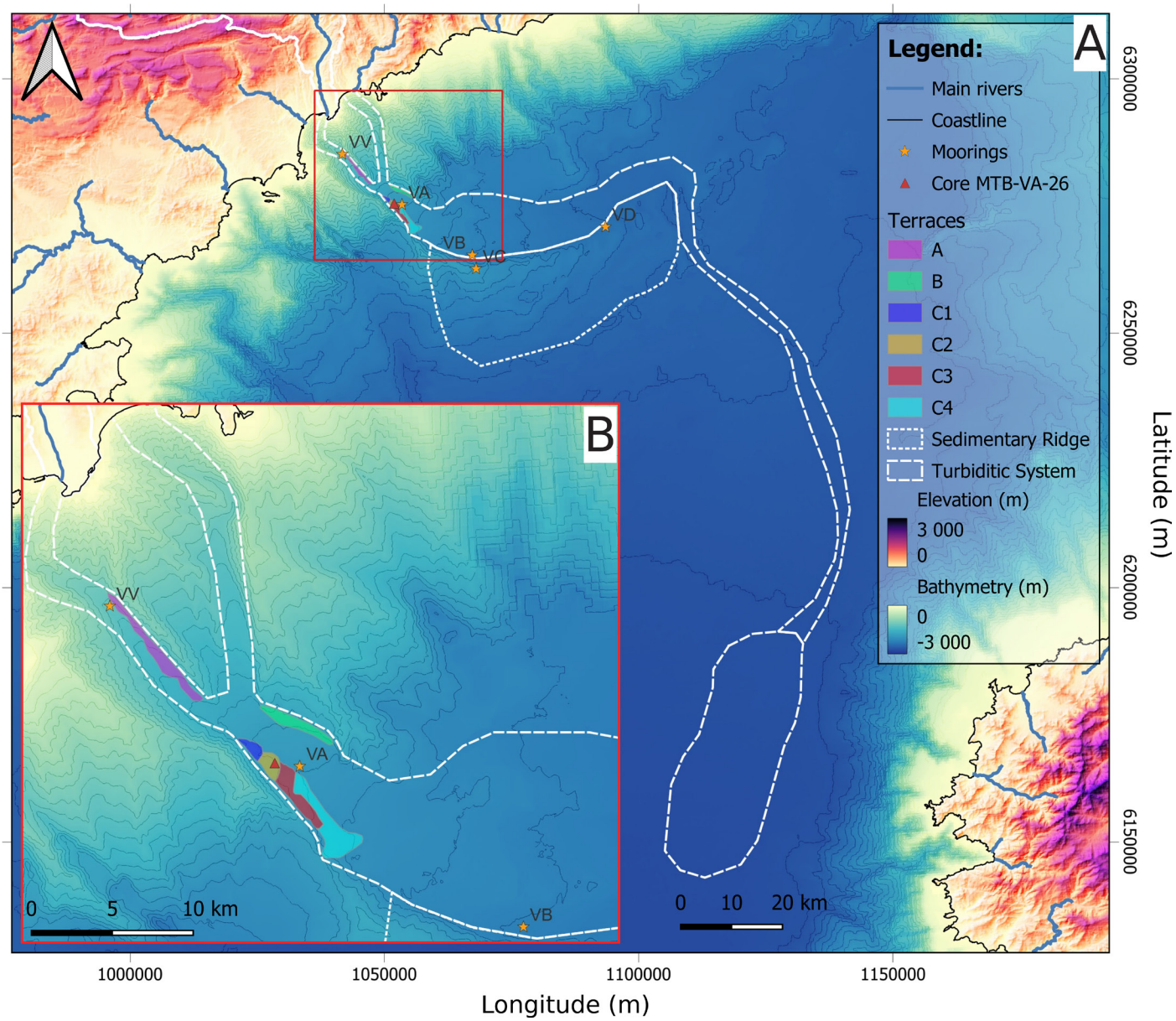


**Figure 5 |** (A) Map of the Var depositional system. (B) Inset is a zoom on the terraces formed by different turbidite events (observations from Mas, 2009; Khripounoff et al., 2009). Bathymetry is from EMODnet with contours at 100 m intervals within the deeper marine setting, and projection is Lambert93.

have a turbidite origin. The hypothesis is that these turbid events are respectively the deposits of the three hyperpycnal currents recorded at mooring VA linked to the floods of the Var River over the same period, where the deposit related to the turbidity current of the 25th September 2006 generated a 4 mm-thick deposit (Mas, 2009). Results of core analysis MTB-VA-02 suggest an average porosity of 72.66% for the top two centimetres (Guidi-Guilvard, 2006).

### 2.3.3. Turbidity current

Each mooring was equipped with a particle trap, located 20 m above the sea floor and designed to collect particles transported in suspension at that level. The particle traps are of cylindrical type with a 0.05 m² surface area and are deployed in the canyon and the Upper Var Valley influenced by high energy flows (VV, VA in Figure 2). The sampling period for these traps is 9 days (Mas, 2009). The average daily particle flux is estimated by dividing the total collected sediment mass by the number of collecting days.

Particle grain sizes measured from the clayey-silt sediment fractions of two flow events show a $D_{50}$ of 10 µm and a $D_{90}$ of around 50 µm (Mas, 2009). The particle flux calculated from the trap associated with the 25th September event is 462 g/m²/day, estimated to be equivalent to 400,000 t of sediment entering the Var system during this event (Mas, 2009). This estimate assumes that a plunging flow occurs when the suspended sediment concentration exceeds 5 kg/m³ (Parsons et al., 2001). Using the rating curve of Laurent (1971), this can be related to a water discharge of 306 m³/s. This field data estimate will be compared to calculations for the volume of suspended material at the outlet of the Var using the model CAESAR-Lisflood. The estimate of the sediment yield from the Var will also be compared to the initial condition required within the model CATS to generate a turbidity current that has the observed characteristics (Figure 4). Deposition will be constrained with the thickness observed at MTB-VA-26 (4 mm; Figure 5).

## 3. Modelling methods

In the hydrology and geomorphology communities, there are two strands of modelling approaches to understanding the impact of run-off on the sediment flux out of the catchment. One approach is to model the water flow, considering the full complexities of the shallow water equations to target the short-timescale flow of the flood wave down the system. For example, the numerical models KLEM (Kinematic Local Excess Model, Borga et al., 2007) and TELEMAC-2D (Broich et al 2019; Ligier 2016) have been used to model the response of the Var and Vésubie catchments to Storm Alex in 2020 (Brigode et al., 2020; Yassine et al., 2020). These two models solve for the Saint-Venant shallow water equations, and they have been applied in relation to the observed distribution of flood damage and the recorded river gauge height. However, while these models capture the fine details of the flood hydrogram, they include neither the transport of sediment nor the resulting change in topography due to the landscape erosion.

In the geomorphology community landscape evolution models (LEMs) such as LAPSUS / LAPSUS-D (Keesstra et al., 2014; Schoorl et al., 2002) and CAESAR-Lisflood (Coulthard et al., 2013) have been developed based on a reduced set of rules to capture the erosion and transport of sediment as a function of run-off. We will focus on CAESAR-Lisflood as it offers a compromise between the simplicity of a rule-based model while retaining a simple solution of the diffusive-wave approximation to the Saint-Venant shallow water equations. This model uses the water flux to estimate the shear stress on the riverbed to calculate the flux of sediment transported down the system. This makes it an ideal model to test the potential range of sediment fluxes eroded from the catchment during rainfall events.

For turbidity currents, there is a similar contrasting approach to modelling the flow of sediment downslope, from solving the full Navier-Stokes equations (Basani et al. 2014; Nasr-Azadani & Meiburg, 2014) to reducing the problem to a set of rules to route sediment downslope (Teles et al., 2016). As for the marine domain of the catchment, we will focus on the process-based model CATS (Teles et al., 2016) to explore under what conditions the sediment release due to storm run-off might create a turbidity current.

In order to apply these models to the natural landscape, we need to pre-process the topographic information to remove artefacts and physical barriers, such as bridges, from the DEM (see Supplementary Material). We also need to reduce the complexity of the input precipitation and sedimentary signals. Therefore, we will first outline the model assumptions, followed by the model results.

### 3.1. Source model – Caesar-Lisflood

To model the transport of sediment within the source catchment, the Var watershed, we use the LEM Caesar-Lisflood (Coulthard et al., 2013). This code is well documented, however in this section we will briefly describe the important modules that affect the precipitation to run-off calculation and the run-off to sediment transport relationship. For each cell in the model domain, the precipitation that falls on that cell is transferred into a run-off assuming some quantity is temporally stored within the subsurface. This conversion is made using the relationships developed as part of TOPMODEL (Beven et al., 1984). The runoff is then routed down the hydraulic slope using a finite difference solution for the shallow water equations where the advective terms are assumed insignificant and can be ignored (Bates et al., 2010). A limitation of this approach is that it is inappropriate for steep slopes. To overcome this limitation, if the flow exceeds an imposed Froude number limit, it is limited to this Froude number. The flowing water then transports sediments. Bedload is transported to the neighbouring cell without taking into account a fall velocity, rather it is transported in the direction of slope (Coulthard et al., 2013). Suspended sediment is transported with the water flux depending on a fall velocity and the water depth (van de Wiel et al., 2007). The flux of suspended material is calculated from a series of empirical functions to convert the model water depth and flux to a basal shear stress and sediment flux. The calculation of the sediment flux is particularly sensitive to the Manning's roughness parameter, as we will outline below. The shear stress $\tau$ is calculated as:

$$\tau = \rho C|u|^2 \quad \text{(Equation 1)}$$

Where $\rho$ is the water density, u is the water velocity, and the friction coefficient, C, is calculated using the Manning-Strickler empirical formula,

$$C = gn^2h^{-1/3} \quad \text{(Equation 2)}$$

Where g is the acceleration due to gravity, n is Manning's roughness coefficient, and h is the water depth. The shear velocity is then calculated as:

$$u_* = (\tau/\rho)^{1/2} \quad \text{(Equation 3)}$$

From the shear stress and shear velocity, the empirical relationship of Wilcock & Crowe (2003) can be used to calculate a sediment flux, $q_s$, for each grain size class, i:

$$q_{si} = \frac{(F_i u_*^3 W_i^*)}{(s-1)g} \quad \text{(Equation 4)}$$

Where s is the specific gravity of the sediment particle, $F_i$ is the proportion of the grain size within the total grain size distribution. The self-similar relationship for each grain size, $W_i^*$, is based on a power law of the ratio of the shear stress to a reference shear stress, $\tau_{ri}$, for each grain size

and is related to the ratio of the grain size and the mean grain size in the bed:

$$\frac{\tau_{ri}}{\tau_{rm}} = \left(\frac{D_i}{D_m}\right)^b \quad \text{(Equation 5)}$$

Where $D_i$ is the grain size diameter, $D_m$ is the median grain size within the distribution of grains within the bed, and $\tau_{rm}$ is the reference shear stress for the median grain size. The exponent b is given by:

$$b = \frac{0.67}{1 + e^{1.5 - D_i/D_m}}$$

In addition, the reference shear stress for the median grain size is calculated as:

$$\tau_{rm} = 0.021 + 0.015e^{-20F_S}$$

Where $F_S$ is the fraction of sand within the grain size distribution on the bed. Finally, depending on the ratio of shear stress to the reference shear stress:

$$W_i^* = 0.002(\tau/\tau_{ri})^{7.5} \text{ if } \tau/\tau_{ri} < 1.35 \quad \text{(Equation 6)}$$

And:

$$W_i^* = 14\left(1 - \frac{0.894}{(\tau/\tau_{ri})^{0.5}}\right)^{4.5} \text{ if } \tau/\tau_{ri} \geq 1.35 \quad \text{(Equation 7)}$$

Therefore, from the empirical sediment transport law, Equation 4, Manning's number impacts the sediment flux via the shear stress ($q_s \propto n^3$) and $W_i^*$. To demonstrate the impact of a change in Manning's number on the sediment flux, we will make the simplifying assumption that $D_i / D_m = 1$ and $F_S$ is large so that $\tau_{ri} = \tau_{rm} = 0.021$. For example, if we assume a water velocity of 0.2 m/s and flow height of 1 m, the sediment flux difference is two orders of magnitude between a Manning's number of $n = 0.015$ and $n = 0.025$.

The detachment and transport of sediment within the Var is variable and a function of the lithology. For example, the "Terres Noires" lithology has a larger *erodibility* compared to other lithologies within the Var. However, one limitation of the version of CAESAR-Lisflood that we use (i.e., the C++ version that is cross platform compatible) is that we do not have spatially variable Manning's number to allow for a variation in the transport of different lithologies.

## 3.2. Sink model – CATS

### 3.2.1. Key concepts for the model CATS

The flow of a turbidity current can be modelled as a solution to Navier-Stokes equations or the shallow water equations, where it is assumed that the density variation is only in the horizontal direction. Numerical methods to solve these equations under certain limiting assumptions have been created since the 1980s (e.g., Bonnecaze et al., 1993; Parker et al., 1986). The classic approach is to solve for the continuity of mass for both the fluid and sediment, and the momentum. Added complexity comes with including both the entrainment of sediment from the ambient fluid and the balance between the kinetic energy needed to maintain the flow and the viscous dissipation of that energy.

Rather than solving as fully as possible for the balance of mass, energy and momentum, another approach is to develop a process-based model built on local rules. It is within this gap that the process-based model CATS was developed (Salles et al., 2007; Teles et al., 2016). The routing of the turbidity current, the entrainment of sediment, and erosion and deposition are modelled with a set of rules within a grid of regular square polygons. The model CATS is explained within Teles et al. (2016). Hence here we will only briefly describe the important processes. The turbidity current is routed downslope based on achieving local equilibrium for the total potential and kinetic energy of the turbidity current (e.g., d'Ambrosio et al., 2001). This routing considers the potential for the turbidity current to rise over objects. The turbidity current is assumed to have a vertical sediment concentration that follows a Rouse profile (Teles et al., 2016). Deposition of sediment that is in suspension is then taken from the lower fraction of the sediment column, the near bottom concentration, the settling velocity, and the shear stress. When calculating the deposition thickness, the porosity of the sediment layers is included to account for the compaction of the layers after deposition. For the Var system, the porosity is relatively high, 72.66% (Guidi-Guilvard, 2006), and the code is adjusted to accommodate for this. The turbidity current is thus routed downslope while depositing a proportion of the sediment in transport.

### 3.2.2. Turbidity current initiation

The routing of the turbidity current within CATS relies on the calculation of the balance between kinetic energy and potential energy. The speed is a scalar quantity related to the local kinetic energy of the flow which is also described through a scalar "height" representing the flow thickness. Therefore, to initiate the current we need to provide a location for the flow, then give the flow an initial height and speed. The flow height is then maintained at this initial value for the source region of cells for a set period. The sum of the quantity of sediment added over time to maintain this initial source corresponds to the total volume of sediment that can be estimated from the outlet of the catchment using estimations from the moorings.

We placed the source at the top of the Var Canyon over a region one cell wide in the y-direction and 15 cells wide in the x-direction, corresponding to a 200 by 3000 m zone (Figure 2). We then explored a set of scenarios for the duration and height of the initial condition. Based on the serrated nature of the flow with multiple peaks we chose to model three scenarios that cover the observed variation in observed water velocity at mooring VV (Figure 6). We coupled these scenarios with different flow heights,

to create three different turbidity current hypotheses, as summarised in Table 3 and Figure 6.

## 4. Results

The results will be presented in two parts: (1) The results of modelling the source or continental domain: the discharge from the Var catchment. (2) The results of modelling the turbidity current in the sink or marine region.

### 4.1. Water discharge and sediment discharge from the catchment

At the Napoléon III bridge, there is continuous measurement of the flow height that is then converted into water discharge. We use this observation to find the model parameters that generate a good fit. Sensitivity analysis of the two catchments based on the Morris method suggests that the model has a nonlinear and important sensitivity to Manning's roughness (Skinner et al., 2018), which impacts the friction term in the implementation of the surface run-off routing using the Lisflood algorithm. Other parameters appearing to be important are numerical parameters such as those that define the slope at the outlet (e.g., a Cauchy-type boundary is applied where water leaves the model domain), or the minimum value for water flux above which flow is routed. Interestingly Skinner et al. (2018) did not explore the impact of the parameter m that controls the recession curve for the conversion of rainfall into run-off. It is beyond the scope of this study to run multiple trajectories within the Morris method to re-analyse the sensitivity of model parameters at the scale of the Var with the inclusion of the TOPMODEL m-parameter. Instead, we chose to fix the numerical parameters and vary both m and Manning's number n to find the best model fit with the water flux using the Nash-Sutcliffe model efficiency coefficient (Nash & Sutcliffe, 1970; Figure 7).

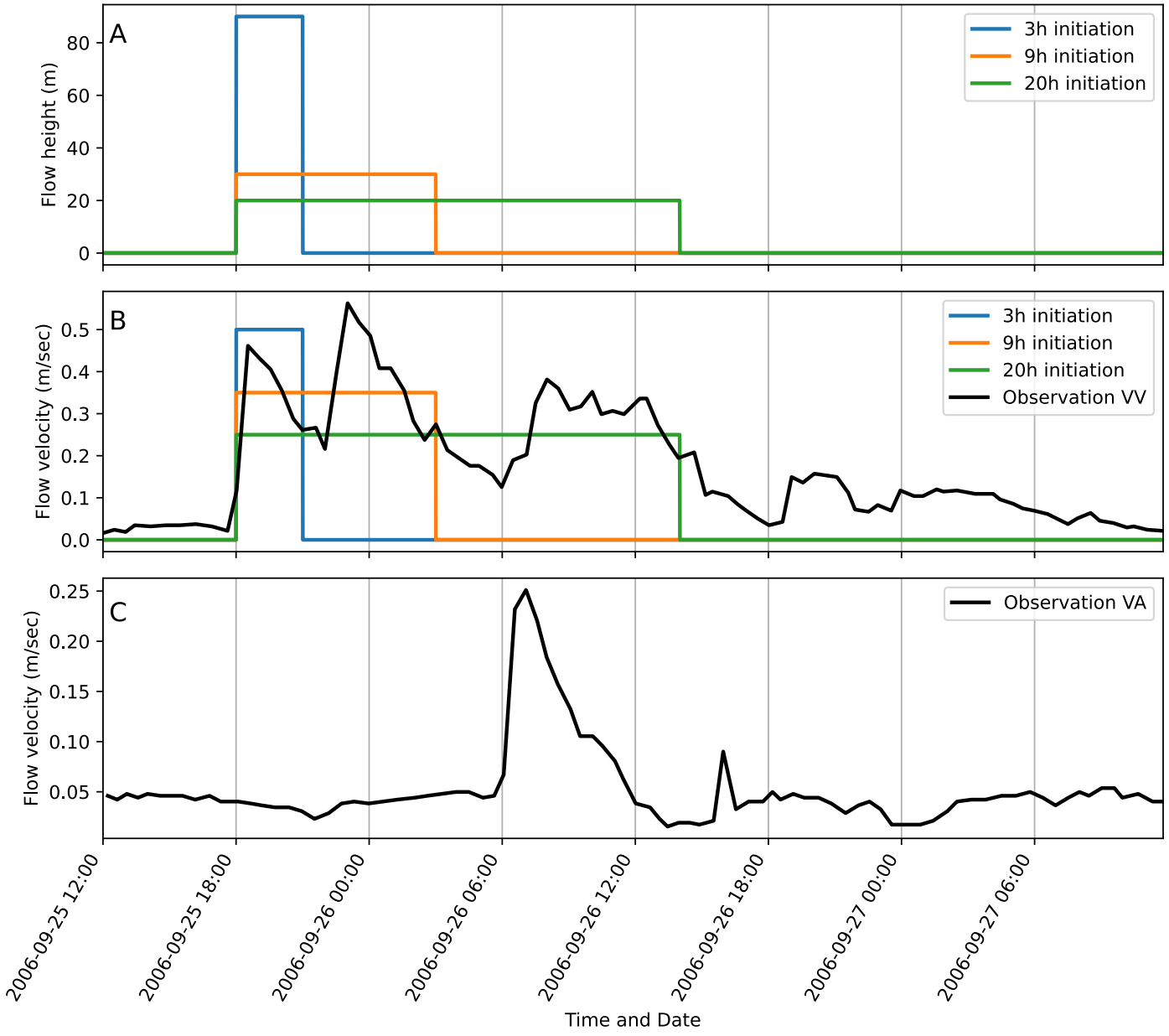


**Figure 6 |** Observed flow velocities at the station VV at 30 m above the sea floor with the three model scenarios for the initial flow at the top of the Var Canyon. (A) Model input flow heights for the three scenarios. (B) Model input flow velocities for the three scenarios and the observed velocity at mooring VV. (C) Observed flow velocity at mooring VA. The observations are from Mas (2009).

| Hypotheses of turbidity current | Initial duration | Mean velocity | Mean height |
|---|---|---|---|
| Surge-type (Pulse1 or 2) | 3h | 0.5 m/s | 90 m |
| Short & moderate (Pulse 1-2) | 9h | 0.35 m/s | 30 m |
| Long & weak (Pulse 1 to 3) | 20h | 0.25 m/s | 20 m |

**Table 3 |** Relative temporal calibration, mean height, and velocities for the three hypotheses for initiation of a turbidity current.

After exploring the model parameter space, we found that there were three key parameters to modify in order to approach the observed water flux. In order of importance, these parameters are (1) water loss before conversion to run-off (evapotranspiration, long-term groundwater storage), (2) TOPMODEL parameter m, and (3) Manning's number n. In the following subsections, we will evaluate the impact of each of these parameters on the model results.

4.1.1. Water loss to evapotranspiration and other pathways

Evapotranspiration (ET) is the loss of water due to both direct evaporation and the uptake by plants and subsequent evaporation. The loss of water to evapotranspiration is typically significant. Water that cycles through ET does not affect the run-off. Furthermore, in the Var system there is potential water loss during the transition from rainfall to run-off in the form of long-term storage in aquifers and groundwater flow within alluvial aquifers, particularly in the plains. These two processes could be included with additional empirical laws and parameters; however, this would lead to increased complexity of an already poorly-defined problem. We therefore chose to reduce the precipitation to give an effective precipitation that is then transferred into run-off. To explore the effect, we reduced precipitation from 50% of the observed rates to 30%. The model output is compared to the discharge time series, and the Nash-Sutcliffe model efficiency (NSE) is calculated (Figure 7). A negative NSE value would imply that the model fit is no better than the time-averaged value of observed discharges over the model time series. Using the NSE as a guide, we find that if 40% of the rainfall over the autumn of 2006 is converted to run-off then CAESAR-Lisflood provides a reasonable fit to the observed discharge, as the NSE has the largest value, 0.72, within the range of parameters we tested (Figure 7).

In Figure 8, the time series of water flux and suspended sediment yield is plotted for the two best-fit model scenarios (Figure 7). For both models, the fit is good for the events occurring after the 25$^{th}$ of September, but the fit is very poor for the discharge event in August. This is most likely because the model does not efficiently convert the localized storm of August 2006 into run-off at the outlet. This storm was localized around Nice and the Mediterranean Alps and absent across the more low-lying areas of the catchment into the northeast (Figure 3). Furthermore, the water routing algorithm is not applicable for steep slopes. To avoid numerical instabilities, a flux limiter is applied via a Froude number. This limits the flux to an upper bound regardless of the precipitation input. This will cause the truncation of the transition from rainfall to run-off.

For all other major events, the magnitude of the discharge matched with reasonable accuracy with rainfalls (Figure 8). This is likely due to the larger spatial distribution of these rainfall events making the routing of overland flow more representative, and the fluvial network delivers the water from the whole catchment to the outlet. Model water depths have a maximum of around 5 meters. This maximum depth is located in the main channel of the Var. In the catchment model, there is no return flow from groundwater within alluvial aquifers, and so the flow depth is only due to water that is transformed rapidly from precipitation to run-off and is then transferred straight to the river system. Only the local, at each cell, short-term storage of water modulates the recession curves after the peak in rainfall.

4.1.2. Short-term storage

Recession curves for the transfer of rainfall to run-off are calculated on each cell using an empirical model based on early versions of TOPMODEL. Water retention is controlled by the parameter m, which is related to land type and use (Beven et al., 1984). For a catchment at the scale of the Var, we are limited to applying one value for all cells. As with the loss of water, we modulate this parameter to calculate a value that provides the best fit for the model duration (Figure 7).

We find that either m = 0.013 m, or m = 0.016 m gives a good fit overall (not including the event of August), but the observed recession after each rainfall event does not fit any single m parameter (Figure 8). For the 25$^{th}$ of September event, the observed recession is faster than the model, while for the large discharge event of December 2006, the observed recession is slower than the model. Over a catchment with the size of the Var, this could be a consequence of multiple complexities between the type of soil, the geology, and the localization of precipitation events. In general, the fit is reasonable for a simple reduced complexity model.

4.1.3. Impact of Manning's roughness

The roughness of the bed affects the model in two ways: (1) Routing of surface water considers the friction on the bed via Manning's number; (2) Sediment transport is computed from a function dependent on the Manning's number. Variation of Manning's number between 0.015 and 0.020 has almost no impact on the fit to the water

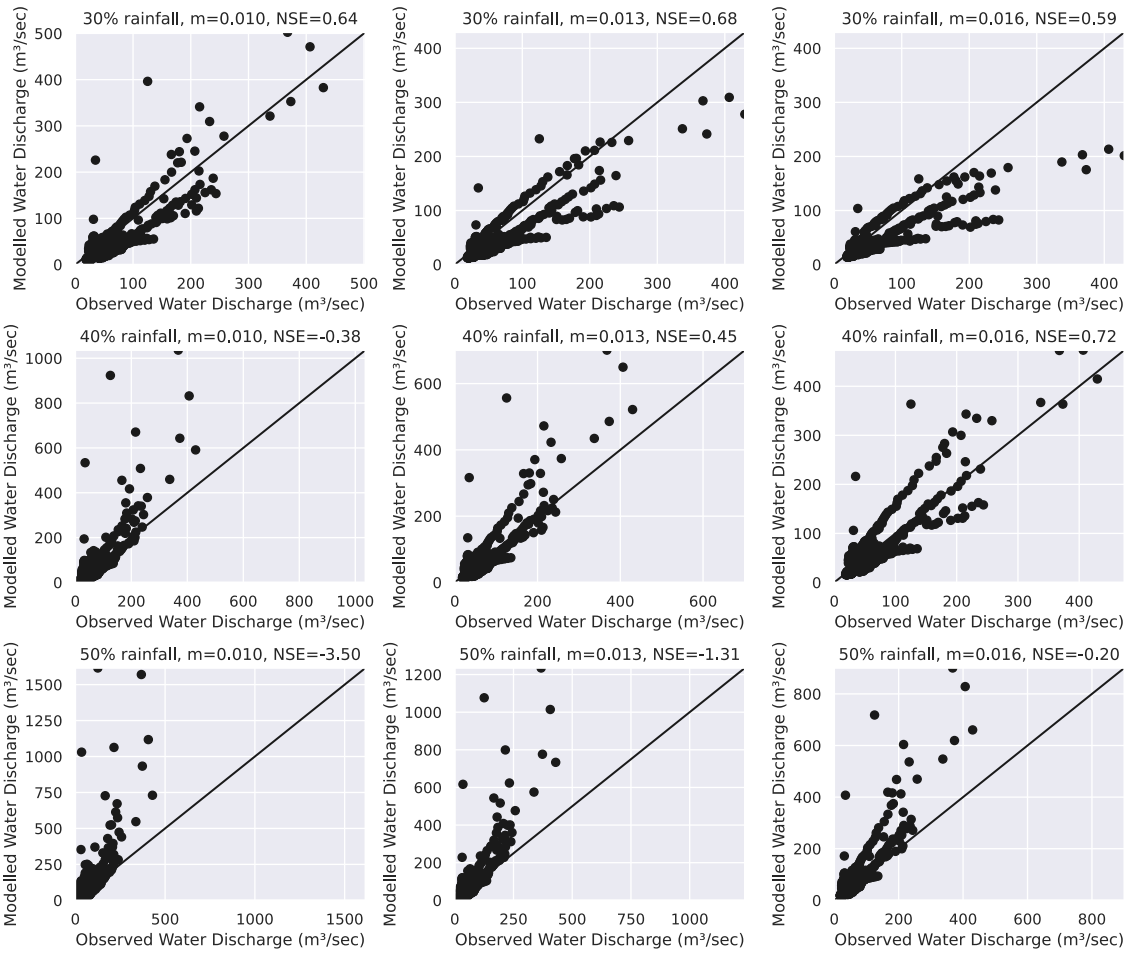


**Figure 7 |** Comparison between observed and modelled water discharge at the outlet, with the Nash-Sutcliffe model efficiency (NSE) displayed. We have varied the percentage of the input rainfall assumed not to be taken up by evapotranspiration and the TOPMODEL m-parameter that controls the peak run-off and recession curve. In these models, the Manning's roughness is 0.02.

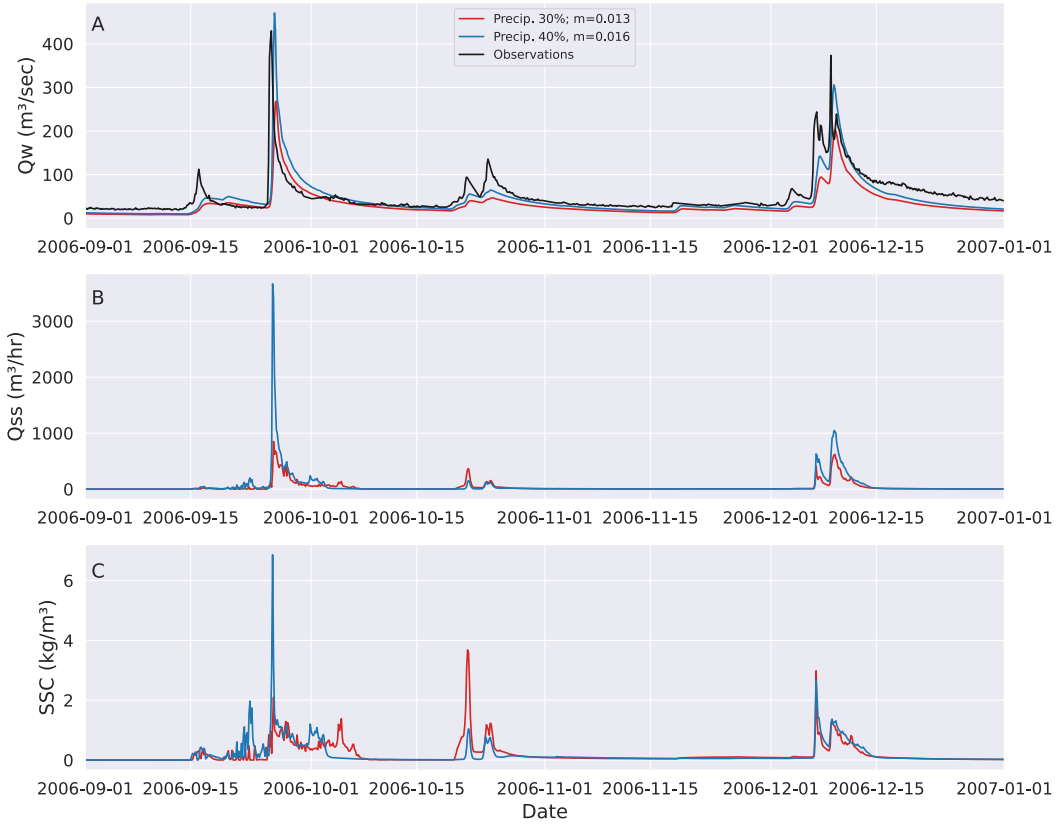


**Figure 8 |** Modelled water and sediment flux for the two models with NSE of 0.72 and 0.68, where the precipitation percentage is 40% and $m$ = 0.016 (NSE = 0.72) and the precipitation percentage is 30% and $m$ = 0.013 (NSE = 0.68). In these models, the Manning's roughness is 0.02. (A) Water flux ($Q_w$) at the outlet for the two scenarios and the observation at the Napoléon III Bridge for comparison. (B) Suspended sediment discharge ($Q_{ss}$) as a volume rate. (C) Concentration of suspended (SSC) material as a density.

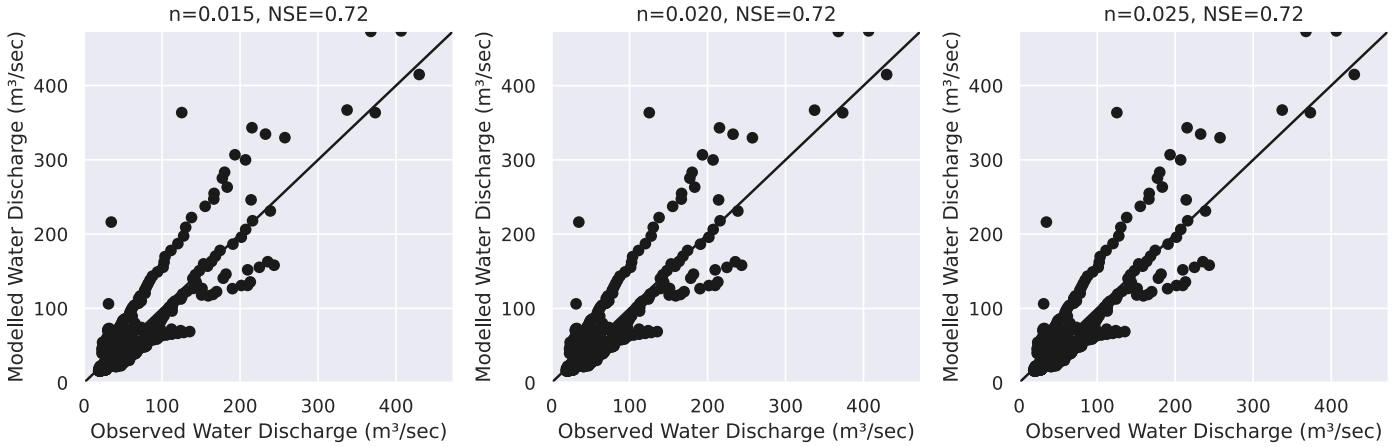


**Figure 9 |** Comparison of the modelled and observed water discharge for a precipitation percentage of 40%, $m$ = 0.016, and a range of Manning's roughness coefficients, $n$ = 0.015 to $n$ = 0.025. It can be seen that the modelled water discharge results are essentially identical.

discharge (Figure 9). However, there is a very large change in the estimated amount of suspended sediment discharged from the catchment (Figure 10). If n = 0.025, then the peak in suspended sediment discharge from the 25th of September event is up to 60,000 m³/h, while if n = 0.020, the peak is around 3000 m³/h. This difference is an order of magnitude; the model is very sensitive to the assumed roughness. Considering Equation 1 to Equation 7, this sensitivity is not surprising, as the sediment flux is related to the cube of the shear velocity, which in turn, directly relates to Manning's roughness.

For the turbidite event of the 25th of September, an estimated 400,000 t of sediment entered the Var depositional system over a period of 19 h (Mas, 2009). If we assume that the density of this material is 2650 kg/m³, then the volume of material is of the order of 151,000 m³. To calculate the volume of material released, we integrate the suspended sediment flux for the whole response to the 25th of September event. For a Manning's roughness of n = 0.015, we find that 23,000 m³ of suspended sediment is exported from the catchment. For n = 0.020, 144,000 m³ of sediment is exported, while for n = 0.025, 4,534,000 m³ of sediment is exported. Based on these calculations, the model that provides the best fit to the estimate for the volume of material exported to the Var depositional system is for n = 0.020, m = 0.016, and 40% of the precipitation enters the soil and is transferred into run-off (Figure 8, blue line).

### 4.2. Turbidity current

The turbidity current is initiated at the top of the Var Canyon system by maintaining a height and velocity within a range of model cells (see Table 3 and Table 4). An input flux of sediment is implicitly applied in order to maintain the flow height and velocity. The goal of the following models was to understand which initial flow conditions would match the delay observed between the two moorings, VV and VA, and can deposit 4 mm of fine-grained sediments at location MTB-VA-6 (Figure 5).

Using an initial flow height of 30 m, an initial velocity of 0.35 m/s, and a duration of 9 h, we find that the flow gains in height as it flows down the Var Canyon, with a peak height of 85 m, 6 h after initiation (Figures 11 and 12) and the turbidity current has arrived at point VA after 12 h. The flow velocity also increases up to 0.74 m/s as it flows down the canyon. We use the point at which the model flow height exceeds 30 m at moorings VV and VA to compare with the observed time difference between these two locations (Figure 11).

If the initial flow height is 90 m, the initial velocity is 0.5 m/s, and the duration is 3 h, we find that the modelled turbidity current passes at mooring VV after 4h42 and at VA after 9h15 (Table 4). We can see that the flow instantly gains speed and height as it flows downslope (Figure 12), with flow velocities at VV that are initially close to 0.9 m/s, and then decrease to 0.6 m/s. This flow velocity increase is due to the steep slopes. The delay between the moorings VV and VA is 6h50 and the current passes through mooring VA

| Initial Volume Concentration (ppm) | Initial Height (m) | Initial Duration (h) | Initial Velocity (m/s) | Time to reach VV (h) | Time to reach VA (h) | Time difference VV to VA (h) | Thickness deposited at MTB-VA-26 (mm) | Input sediment volume (m³) |
|---|---|---|---|---|---|---|---|---|
| 550 | 90 | 3 | 0.5 | 4h42 | 9h15 | 6h50 | 6.85 | 767,282 |
| 550 | 20 | 20 | 0.2 | - | - | - | 0 | 442,365 |
| 750 | 30 | 9 | 0.35 | 9h03 | 7h21 | 11h46 | 5.54 | 721,676 |
| 550 | 30 | 9 | 0.35 | 9h06 | 9h55 | 11h43 | 3.95 | 527,047 |
| 375 | 30 | 9 | 0.35 | 9h10 | 11h24 | 11h36 | 3.11 | 353,259 |

**Table 4 |** Model initial conditions and times of current arrival at moorings VV, VA and deposit thickness at MTB-VA-26.

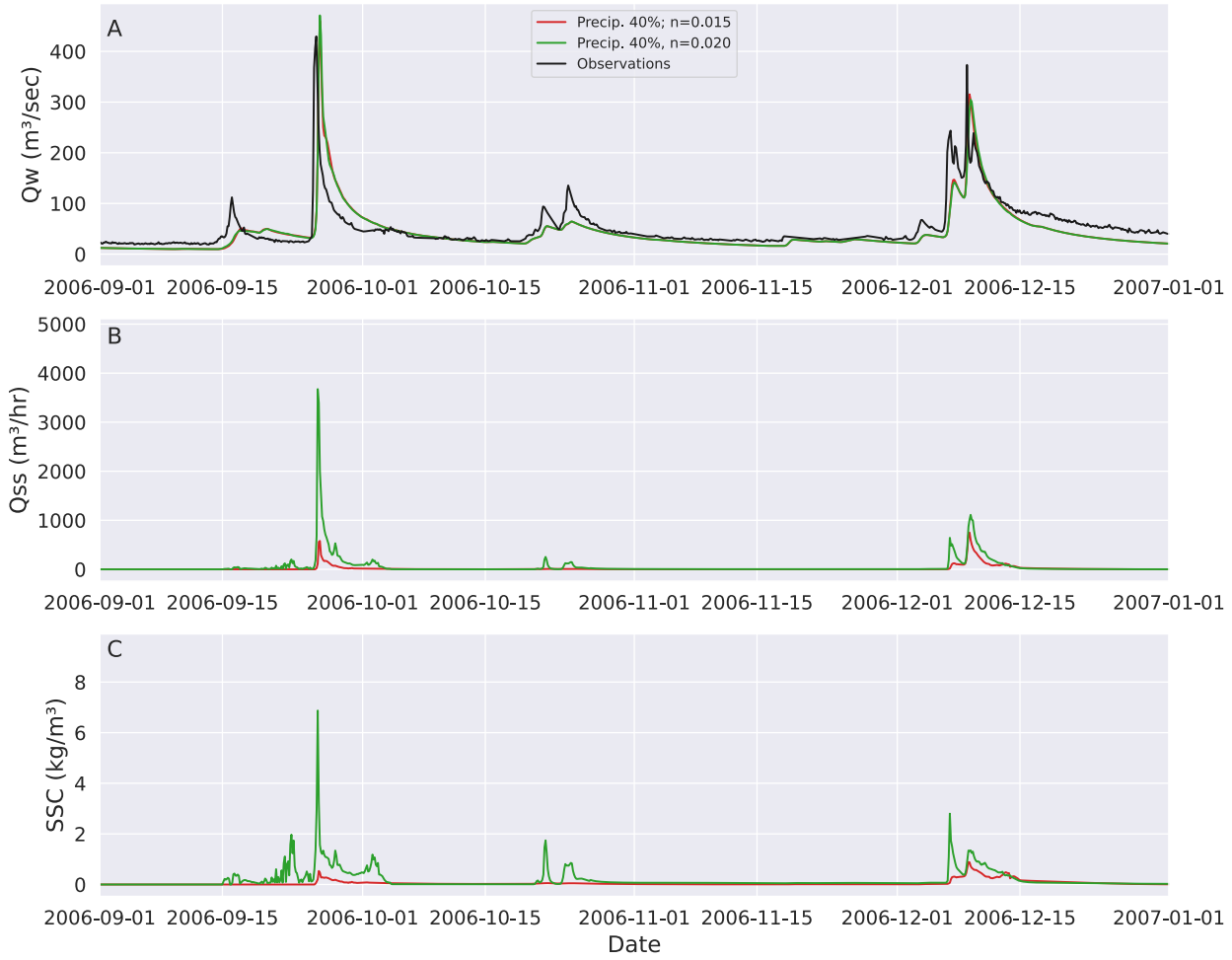


**Figure 10 |** Modelled water flux and suspended sediment yield for three different values of Manning's roughness. There is an order of magnitude difference between $n$ = 0.015 and $n$ = 0.025. (A) Water flux ($Q_w$) at the outlet for the two scenarios and the observation at the Napoléaon III Bridge for comparison. (B) Suspended sediment discharge ($Q_{ss}$) as a volume rate. (C) Concentration of suspended material (SSC) as a density.

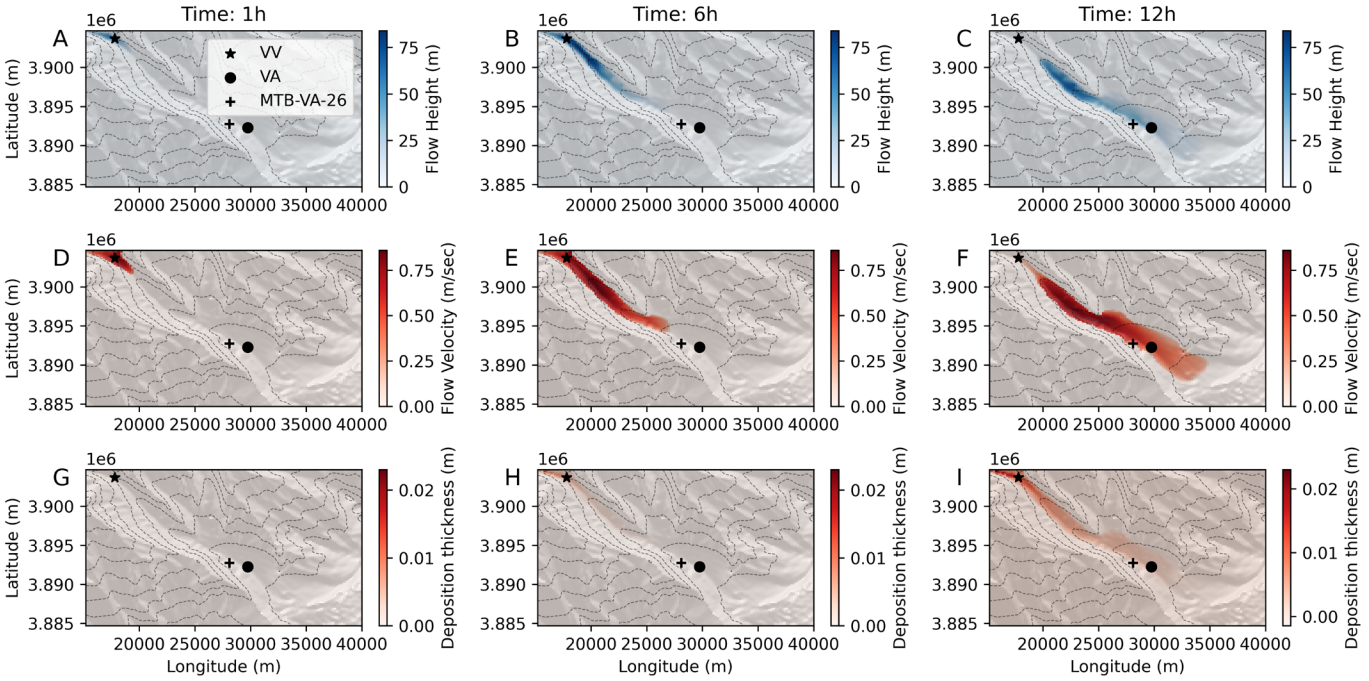


**Figure 11 |** Modelled turbidity current height and velocity at different snapshots in time. The initial flow is defined with an initial flow height of 30 m, an initial velocity of 0.35 m/s, and a duration of 9 h (Table 3). Parts (A, B, C) show flow height after 1 h, 6 h and 12 h, respectively. Parts (D, E, F) show flow velocity after 1 h, 6 h and 12 h, respectively. Parts (G, H, I) show the thickness of the sediment deposits after 1 h, 6 h, and 12 h respectively. The front of the flow reaches the points MTB-VA-26 and VA just after 6 h of model simulation, with the main section of the flow arriving sometime after 12 h since the initiation of the model run. Projection for the maps is Lambert93.

after 9h15 (Table 4). The flow velocity at VA remains high, peaking at 0.8 m/s (Figure 12). These flow characteristics do not match with the observations at VV and VA. The time it takes for the turbidity to reach VA from VV is larger than the record from the mooring. Furthermore, the delay between the moorings VV and VA is too short compared to the observations (Figure 12; Mas, 2009).

We tested the model solution for a low flow height over a long duration. When the initial flow height is 20 m and the velocity is low (0.2 m/s), over a long duration (20 h), the model flow never reaches the height (30 m) of the traps that were deployed to measure the current within the Var (30 m above the seafloor; Figure 12). Furthermore, the flow cannot reach a sufficient height to deposit any sediment on the terrace at location MTB-VA-26 (Table 4). The flow velocity increases from the initial velocity of 0.2 m/s to 0.6 m/s due to the steep slope at mooring VV and reduces to 0.4 m/s at mooring VA (Figure 12).

The third scenario is an initial flow duration of 9 h with a flow elevation of 30 m and velocity of 0.35 m/s. In this case, the flow reaches mooring VV after 9h06 and VA after 9h55 for the same model volume concentration of 550 ppm, similar to the previous model simulations for longer and shorter initial flows (Table 4, Figure 12). In this case, the flow velocity is 0.7 m/s at mooring VV and reduces to 0.5–0.6 m/s at mooring VA. For all these scenarios, the initial concentration remains stable as the flow moves through the two locations, showing that only a small amount of sediment has been lost by deposition or added by erosion (Figure 12).

The initial flow concentration has a small impact on the flow duration at mooring VA, but in all cases, the more concentrated the flow, the shorter the flow duration. A duration of 7h21 is modelled if the volume concentration is elevated at 750 ppm and a duration of 11h24 if the volume concentration is 375 ppm (Table 4, Figure 13). Consequently, at mooring VV, the flow is faster when sediment concentration increases (Figure 13). However, at the observation depth, there is no observable difference in the arrival time of the flow at mooring VA.

Modification of the initial sediment concentration finally has an impact on the quantity of sediment deposited (Table 4). Mas (2009) described that 4 mm of sediment were deposited at location MTB-VA-26. Using several simulations with changing the delay between the time of arrival between moorings VV and VA, the initial duration of the flows, and the quantity of sediment deposited at location MTB-VA-26, the best match with the observations corresponds to an initial flow height of 30 m, a duration of 9 h, and a volume concentration of 550 ppm. For this closest fit, the total sediment input in the model is 527,047 $m^3$.

## 5. Discussion

The source landscape evolution model that best fits the hydrological observations would suggest that during the three days from the 25th to the 27th of September 2006, 144,000 $m^3$ of sediment were exported from the catchment. However, the model is very sensitive to the Manning's roughness parameter, $n$, because the sediment flux is calculated as a function of shear stress. The sink turbidity current model that best fits the observations from sediment traps and the core requires an input sediment flux of 527,047 $m^3$ over a duration of 9 h. Meanwhile, by upscaling the observed sediment quantities within the sediment traps at location VV to a cross-section of the gully, the sediment volume for the turbidity event is estimated to be 151,000 $m^3$ (Mas, 2009).

The estimates from the source model and sink model are of the same order of magnitude. However, the durations over which the source released sediment and the sink received sediment are very different. We will first discuss the implications and uncertainties of the model simulations for the magnitude of sediment, and then discuss the duration of events.

### 5.1. Sediment flux magnitudes

Due to the large number of parameters and the relatively long model run times (model runs can typically take in the range of 6 to 24 h), only the Morris Method has been used to look at the sensitivity of CAESAR-Lisflood to the model parameters (Skinner et al., 2018). A key result is that the Manning number is the parameter that displays the most significant sensitivity. This sensitivity means that in our case the modelled sediment flux can change by two orders of magnitude through only a small modification of the Manning number (Figure 10). Unfortunately, there is no measurement of suspended sediment discharge for the flood event of September 2006. While there are punctual measurements of suspended sediment from 1971 (Laurent, 1971), they are too sparse to rule out the models as the observations do not capture peak water flux events. Therefore, in comparison to the estimates for sediment discharge from the offshore moorings (Mas, 2009) and for a reasonable parameter value for the roughness applied over the whole catchment, $n$ = 0.02, the sediment flux delivered to the basin was likely of the order of $10^5$ $m^3$.

In this study, we use a simple algorithm to model a natural flow of turbidity currents that is significantly more complex. Therefore, the sediment volumes involved must also be interpreted with care, despite the lack of significant model sensitivity to the explored parameters. Natural turbidity currents pass through the two traps with a large head followed by a body and a tail, while modelled flows pass more with a gradual increase in height (Figure 12 and Figure 13). This might mean that the observed turbidity current had a much smaller volume of sediment compared to the modelled flow. Furthermore, only 35% of the total

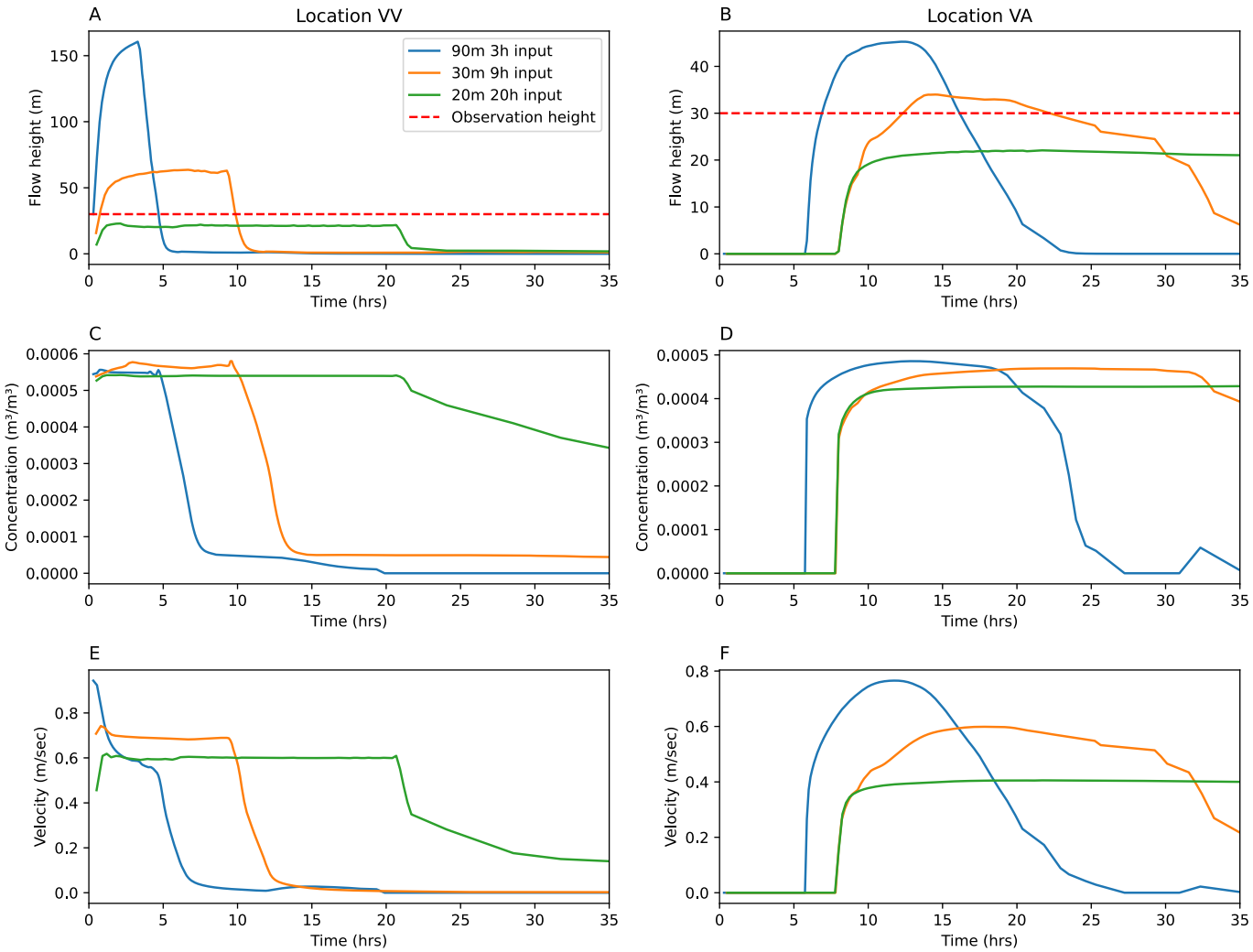


**Figure 12 |** Flow height, concentration, and velocity at the locations VV and VA for the three different scenarios for an initial turbidity current: Blue line – a flow that is initially 90 m high and has a duration of 3 h at the input location (Figure 2). Orange line – a flow that is initially 30 m high and has a duration of 9 h at the input location. Green line – a flow that is initially 20 m high and duration of 20 h (Table 3). (A) Flow height as the turbidity current passes through location VV (see for example, Figure 11). (B) Flow height as the turbidity current passes through location VA. (C) Near bottom sediment concentration at location VV. (D) Near bottom sediment concentration at location VA. (E) Flow velocity of the turbidity current at location VV. (F) Flow velocity of the turbidity current at location VA.

volume of sediment within the model was deposited during the total run time (35 hrs), suggesting that around 65% of the sediment remains in suspension. The model results imply that the relatively dilute turbidity current required to match the observations tends to further dilute within the water and have limited deposition. With these caveats in mind, the modelling results suggest that the basin received the order of $10^5$ $m^3$ of suspended sediment during the September 2006 flood event.

### 5.2. Duration of the input sediment flux

The input sediment flux that best matches the time between the records at moorings is 9 hours long. The observations from the current meter at mooring VV show a rotation to the south and an increased flow of water at 18 h on the 25th of September and then a reduction and rotation to the west at 14 h on the 26th of September. At mooring VA, the flow increases and there is a rotation of the direction at 6 h on the 26th of September, and the flow then reduces and rotates again at 18 h on the same day (Mas, 2009). The velocities measured at 30 m above the seafloor vary from around 0.5 and 0.1 m/s, which is relatively slow compared to estimates for the velocity of turbidity currents (Piper & Savoye, 1993) and the current generated by slope failure in 1979 (Gennesseaux et al., 1980). The low velocities are consistent with concentrations much lower (less than 1 %) than the 6-9% concentration of the flow related to the 1979 Nice event (Piper & Savoye, 1993). The velocity of a turbidity current is larger at the base and decreases upward (e.g., Talling et al., 2023). In the model CATS, there is only a uniform vertical velocity for the routing algorithm. Therefore, the magnitude of the modelled and observed velocities are not directly comparable. However, the delay between the arrival of the turbidity current at VV and VA is used as an indicator for the matching between the model and the natural current. Furthermore, the quantity of sediment deposited can be used as a second calibration parameter for the model. For these two measurements, a 9 hour initial current gave the best fit.

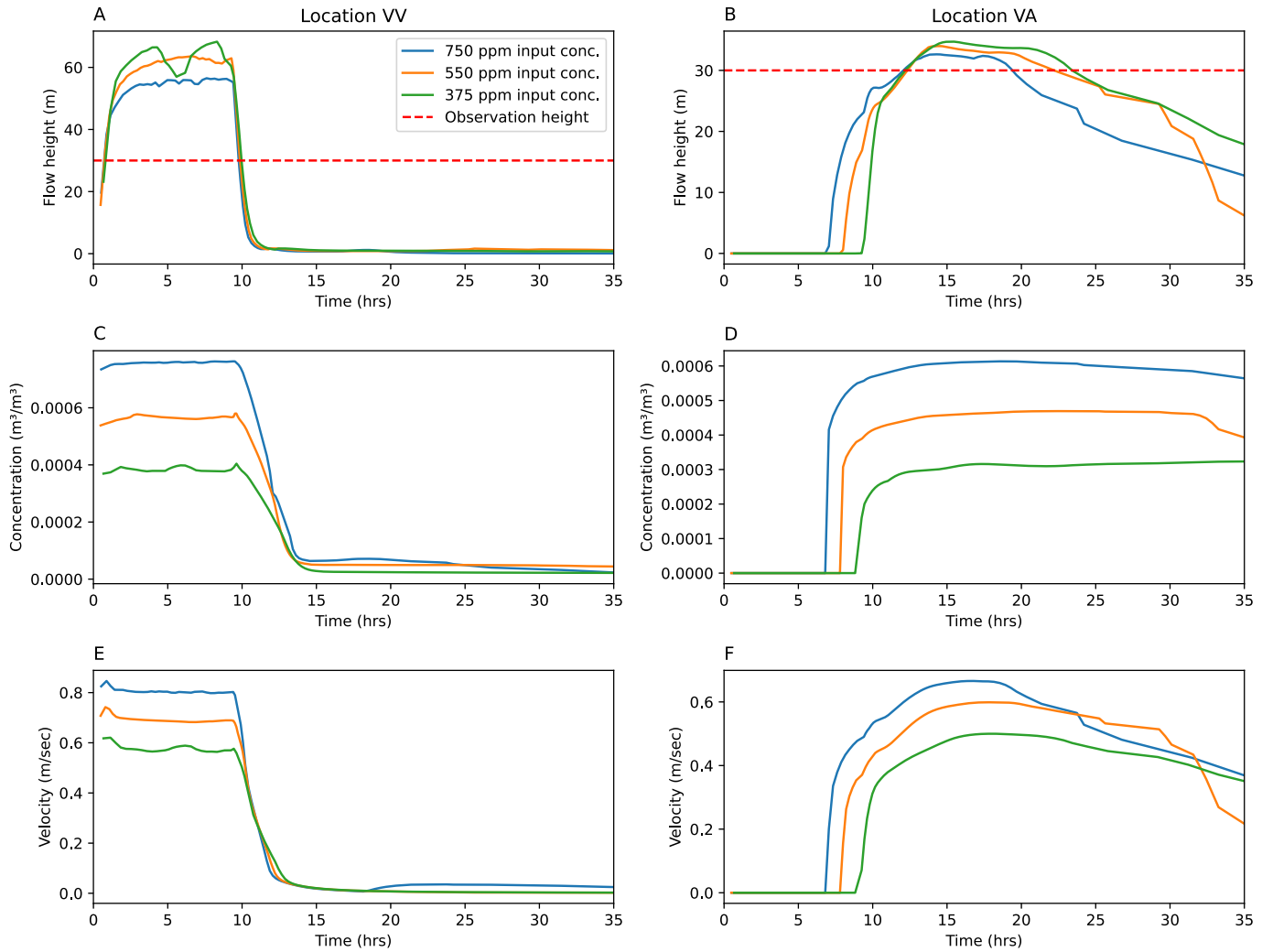


**Figure 13 |** Flow height, concentration, and velocity at the locations VV and VA for flow height, concentration, and velocity at the locations VV and VA for the three different initial sediment concentrations for an initial turbidity current that is initially 30 m high and has a duration of 9 h at the input location (Figure 2): Blue line – input sediment concentration of 750 ppm. Orange line – input sediment concentration of 550 ppm. Green line – input sediment concentration of 375 ppm (Table 3). (A) Flow height as the turbidity current passes through location VV (see for example Figure 11). (B) Flow height as the turbidity current passes through location VA. (C) Near bottom sediment concentration at location VV. (D) Near bottom sediment concentration at location VA. (E) Flow velocity of the turbidity current at location VV. (F) Flow velocity of the turbidity current at location VA.

The two models would suggest that the turbidity events of the autumn of 2006 were driven by a plunging flow from the sediment released from the Var River mouth and were slow moving and diluted. The Var Canyon provides a geological record of turbidity currents history. During the Pleistocene, the sedimentary record would suggest that numerous sand and mud-rich turbidity currents flowed down the canyon system (Piper & Savoye, 1993). Turbidity currents drastically increased during Marine Isotope Stage (MIS) 2 (Var Levee, Bonneau et al., 2014) and nearly stopped during the Holocene. These currents likely travelled slowly with speeds of around 0.35 m/s and are inferred to be caused by the increased sediment discharge of the Var system during a cold period (Piper & Savoye, 1993). Mulder et al. (2001) also showed that deposits in core KV10 located on the terrace farther downstream in the canyon, correlate well with river floods with a discharge above 1227 $m^3/s$ and an estimated return period of 5–5.5 y, similar to the September 2006 flood event. From the sediment grain size, these authors inferred low competency and low velocity flows. We can therefore infer that when turbidity currents are directly generated by floods (hyperpycnal flows), turbidity currents have velocities that are less than 1 m/s (Gennesseaux et al., 1971; Mas, 2009). The low sediment concentrations predicted from the catchment model, 2 to 6 $kg/m^3$ (Figure 8) are indicative of turbidity currents initiated by settling of suspended sediment (Parsons et al., 2001).

The two models imply that the long duration river flood event is transformed into a shorter duration turbidity event. The connectivity between river floods that deliver dilute sediment quantities, and the generation of turbidity currents is not clear (Talling et al., 2023), with observations from evidence pointing to secondary processes such as sediment trapping within the estuary and mobile mud layers that lead to the generation of a turbidity current (Hage et al., 2019). However, these dilute turbidity currents form in areas with a tidal range. In the Var estuary, the tidal range is low yet storm-related wave generation at the

coast could potentially help trigger the shorter duration turbidity currents. Therefore, we tentatively propose that the day-long flood event is transformed into a half-day-long turbidity current via the interaction between the river output and the storm wave action. This current then deposits less than half of its sediment load, and the rest is dispersed into the Mediterranean Sea mixing with hemipelagic sedimentation.

### 5.3. Implications for source-to-sink connectivity

The results from the two models imply that flood events can deliver large quantities of suspended sediment to the basin over a very short period of time, yet only a fraction of the sediment delivered to the basin is deposited in the canyon system and on the continental rise by plunging hyperpycnal turbidity currents. The remainder is spread under the form of a surface (hypopycnal) plume and the particles are further transported by surface currents into the distal parts of the marine basin. In the Var case, the shortness of the continental shelf does not allow for significant storage close to the river mouth. Hyperpycnal flows form only when sediment concentration at the Var River mouth is in the order of 2 to 6 kg/m$^3$. For the rest of the time, sediments may plunge by convective sedimentation or are spread away.

Turbidity currents are thought to be a very important pathway for the transport of particulate organic carbon, pollutants within the suspended load and in particular macro and microplastics to the deep sea (Kane et al., 2020; Talling et al., 2023). However, over the time period modelled in this study, i.e., from August 2006 to January 2007, only two rainfall events generated enough sediment yield to pass the threshold for a plunging flow and the generation of a turbidity current. Therefore, a quantity of suspended sediment, microplastics and other particulate material might be transported out into the oceans by surface plumes to later degrade and sink into the deep ocean. Finally, if accumulation is only by events that exceed a certain threshold, then models should be guided by the frequency of high-intensity precipitation events, rather than the mean precipitation rates.

## 6. Conclusions

This work aimed to explore if the source-to-sink system of the Var could be modelled using two reduced complexity models: CAESAR-Lisflood for the source catchment, and CATS for the sink. We find that the model CAESAR-Lisflood is highly sensitive to the assumed surface roughness (Manning's number). The sediment discharge varies by an order of magnitude when n is changed from 0.015 to 0.020, which is explained by the assumed relationship between the water flux and the shear stress on the bed. Using estimates of sediment discharge from the Var Canyon we can find a best fitting source model that matches the main features of the observed response of the Var system to significant rainfall events in the autumn to winter of 2006. The two models combined imply that when the suspended sediment yield is above a threshold concentration of 2 to 6 kg/m$^3$, corresponding to a water discharge of 300 m$^3$/s, a plunging flow will form to generate a turbidity current. The day-long flood discharge is transformed into a shorter-lived turbidity event as the suspended load destabilises within the water column. The models then imply that one third of the sediment within the turbidity current is deposited locally within the canyon system. Two thirds of the suspended material enters the marine sink as a hypopycnal plume and is transported far into the marine sink.

## Acknowledgments

We would like to thank the editor Ian Kane, the anonymous reviewer and Elda Miramontes for their comments that greatly improved this manuscript. We would also like to thank Romain Vaucher for guiding the manuscript from submission to publication.

## Authors contribution

Arthur Remaud: methodology, formal analysis, investigation, data curation, writing – original draft. John Armitage: methodology, formal analysis, investigation, writing – original draft, supervision. Vanessa Teles: methodology, writing – review and editing, supervision. Sébastien Rohais: methodology, writing – review and editing, supervision. Thierry Mulder: writing – review and editing.

## Data availability

This manuscript has supplementary material that describes how we processed the DEM for the modelling of the source catchment. The landscape evolution model CAESAR-Lisflood is available here, https://github.com/dvalters/HAIL-CAESAR, and the DEM pre-processing methods can be found here, https://github.com/johnjarmitage/caesarPy/tree/master/dem-preprocessing. The turbidity current model CATS is currently not open source as it is built upon the IFP Energies nouvelles C++ library ArcGeoSim, which has not yet been released for open source.

## Conflict of interest

There are no conflicts of interest.

## References

Anthony, E. J. (1995). Impacts géomorphologiques côtiers des aménagements du Var et de son delta, Côte d'Azur, France. Hommes Et Terres Du Nord, 1(1), 73–81. https://doi.org/10.3406/htn.1995.2493

Anthony, E. J., & Julian, M. (1999). Source-to-sink sediment transfers, environmental engineering and hazard mitigation in the steep Var River catchment, French Riviera, southeastern France. Geomorphology, 31(1-4), 337–354. https://doi.org/10.1016/S0169-555X(99)00088-4

Basani, R., Janocko, M., Cartigny, M.J.B., Hansen, M., & Eggen huisen, J.T. (2014). MassFLOW-3D as a simulation tool for turbidity currents: some preliminary results. In A. W. Martinius, R. Ravnås, J. A. Howell, R.J. Steel, & J.P. Wonham (Eds.), From Depositional Systems to Sedimentary Successions on the Norwegian Continental Margin (pp. 587–608). International Association of Sedimentologists, Special Publication 46.

Bates, P. D., Horritt, M. S., & Fewtrell, T. J. (2010). A simple inertial formulation of the shallow water equations for efficient two-dimensional flood inundation modelling. Journal of Hydrology, 387(1-2), 33–45. https://doi.org/10.1016/j.jhydrol.2010.03.027

Beven, K. J., Kirkby, M. J., Schofield, N., & Tagg, A. F. (1984). Testing a physically-based flood forecasting model (TOPMODEL) for three U.K. catchments. Journal of Hydrology, 69(1-4), 119–143. https://doi.org/10.1016/0022-1694(84)90159-8

Bonneau, L., Jorry, S. J., Toucanne, S., Silva Jacinto, R., & Emmanuel, L. (2014). Millennial-Scale Response of a Western Mediterranean River to Late Quaternary Climate Changes: A View from the Deep Sea. The Journal of Geology, 122(6), 687–703. https://doi.org/10.1086/677844

Bonnecaze, R. T., Huppert, H. E., & Lister, J. R. (1993). Particle-driven gravity currents. Journal of Fluid Mechanics, 250, 339–369. https://doi.org/10.1017/S002211209300148X

Borga, M., Boscolo, P., Zanon, F., & Sangati, M. (2007). Hydrometeorological analysis of the 29 August 2003 flash flood in the Eastern Italian Alps. Journal of hydrometeorology, 8(5), 1049–1067, https://doi.org/10.1175/JHM593.1

Brigode, P., Bourgin, F., Yassine, R., Delestre, O., & Lagrée, P. Y. (2020). Are Hydrologic-Hydraulic Coupling Approaches Able to Reproduce Alex Flash-Flood Dynamics and Impacts on Southeastern French Headwaters? In P. Gourbesville & G. Caignaert (Eds.), Springer Water. Advances in Hydroinformatics: SimHydro 2019 - Models for Extreme Situations and Crisis Management (1st ed. 2020, pp. 419–436). Springer. https://doi.org/10.1007/978-981-19-1600-7_27

Broich, K., Pflugbeil, T., Disse, M., & Nguyen, H. (2019). Using TELEMAC-2D for Hydrodynamic Modeling of Rainfall-Runoff. Proceedings of the XXVIth TELEMAC-MASCARET User Conference 2019, Toulouse, France (pp. 15–17). https://doi.org/10.5281/zenodo.3611524

Chapuis, M., Ait Elabas, A., Souriguére, K., Compagnon, F., Mayen, V., & Terrier, B. (2018). Quantification of the morpho-dynamics and ecological functionality of a Mediterranean river. In A. Paquier & N. Rivière (Eds.), River Flow 2018 - Ninth International Conference on Fluvial Hydraulics, 40, 2042. E3S Web of Conferences https://doi.org/10.1051/e3sconf/20184002042

Coulthard, T. J., Neal, J. C., Bates, P. D., Ramirez, J., Almeida, G. A. M. de, & Hancock, G. R. (2013). Integrating the LISFLOOD-FP 2D hydrodynamic model with the CAESAR model: implications for modelling landscape evolution. Earth Surface Processes and Landforms, 38(15), 1897–1906. https://doi.org/10.1002/esp.3478

D'Ambrosio, D., Di Gregorio, S., Gabriele, S., Gaudio, R. (2001) A Cellular Automata model for soil erosion by water. Physics and Chemistry of the Earth, Part B: Hydrology, Oceans and Atmosphere, 26(1), 33-39. https://doi.org/10.1016/S1464-1909(01)85011-5

Ding, X., Salles, T., Flament, N., & Rey, P. (2019). Quantitative stratigraphic analysis in a source-to-sink numerical framework. Geoscientific Model Development, 12(6), 2571–2585. https://doi.org/10.5194/gmd-12-2571-2019

Gennesseaux, M. (1962). Une cause probable des écoulements turbides profonds dans le canyon sous-marin du Var (Alpes Maritimes). Comptes Rendus De L'académie Des Sciences, 254, 2038–2040. https://gallica.bnf.fr/ark:/12148/bpt6k40013/f343.item

Gennesseaux, M., Guibout, P., & Lacombe, H. (1971). Enregistrement de courants de turbidité dans la vallée sous-marine du Var (Alpes Maritimes). Comptes Rendus De L'académie Des Sciences, Séries D, 273, 2456–2459.

Gennesseaux, M., Mauffret, A., & Pautot, G. (1980). Les glissements sous-marins de la pente continentale niçoise et la rupture de câbles en mer Ligure (Méditerranée occidentale). Comptes Rendus De L'académie Des Sciences, Séries D, 290, 959–962.

Gourbesville, P., & Ghulami, M. (2022). Deterministic Modelling for Extreme Flood Events - Application to the storm Alex. In M. Ortega-Sánchez (Ed.), Proceedings of the 39th IAHR World Congress (Online), Granada, Spain (pp. 19–24). International Association for Hydro-Environment Engineering and Research. https://doi.org/10.3850/IAHR-39WC2521716X20221402

Grandjean, G., Pennetier, C., Bitri, A., Meric, O., & Malet, J.-P. (2006). Caractérisation de la structure interne et de l'état hydrique de glissements argilo-marneux par tomographie géophysique : l'exemple du glissement-coulée de Super-Sauze (Alpes du Sud, France). Comptes Rendus. Géoscience, 338(9), 587–595. https://doi.org/10.1016/j.crte.2006.03.013

Guidi-Guilvard, L. (2006). Etude de l'effet de la dynamique sédimentaire sur la méiofaune dans le canyon du Var. Campagne ENVAR 1. IFRAMER. https://archimer.ifremer.fr/doc/00432/54362/

Habib, P. (1994). Aspects géotechniques de l'accident du nouveau port de Nice. Revue Française de Géotechnique, 65, 3–15.

Hage, S., Cartigny, M. J. B., Sumner, E. J., Clare, M. A., Hughes Clarke, J. E., Talling, P. J., Lintern, D. G., Simmons, S. M., Silva Jacinto, R., Vellinga, A. J., & Allin, J.R. (2019). Direct Monitoring Reveals Initiation of Turbidity Currents From Extremely Dilute River Plumes. Geophysical Research Letters, 46, 11310–11320. https://doi.org/10.1029/2019GL084526

Jaeggi, M. (2003). Etude du fonctionnement physique du lit de fleuve Var: Rapport d'Etude (0.81.5561). SMEBVV, Syndicate Mixte d'Etudes de la Basse Vallee du Var.

Kane, I. A., Clare, M. A., Miramontes, E., Wogelius, R., Rothwell, J. J., Garreau, P., & Pohl, F. (2020). Seafloor microplastic hotspots controlled by deep-sea circulation. Science, 368(6495), 1140–1145. https://doi.org/10.1126/science.aba5899

Keesstra, S. D., Temme, A., Schoorl, J. M., & Visser, S. M. (2014). Evaluating the hydrological component of the new catchment-scale sediment delivery model LAPSUS-D. Geomorphology, 212, 97–107. https://doi.org/10.1016/j.geomorph.2013.04.021

Khripounoff, A., Vangriesheim, A., Crassous, P., & Etoubleau, J. (2009). High frequency of sediment gravity flow events in the Var submarine canyon (Mediterranean Sea). Marine Geology, 263(1-4), 1–6. https://doi.org/10.1016/j.margeo.2009.03.014

Laurent, R. (1971). Charge solide en suspension et géochimie das un fleuve cotier Méditerranéen: Le Var (Alpes-Maritimes) [Thése de 3eme Cycle de Sédimentologie]. Université de Nice, Nice.

Liébault, F., Melun, G., Piton, G., Chapuis, M., Passy, P., & Tacon, S. (2024). Channel change during catastrophic flood: Example of

Storm Alex in the Vésubie and Roya valleys. Geomorphology, 446, 109008. https://doi.org/10.1016/j.geomorph.2023.109008

Ligier P.L. (2016). Implementation of a rainfall-runoff model in TELEMAC-2D. Proceedings of the XXIIIrd TELEMAC-MASCARET User Conference 2016, Paris, France (pp. 13–19).

Ma, Q., & Gourbesville, P. (2020). Modelling Strategy of Deterministic Distributed Hydrological Model Development at Catchment Scale. In P. Gourbesville & G. Caignaert (Eds.), Springer Water. Advances in Hydroinformatics: SimHydro 2019 - Models for Extreme Situations and Crisis Management (1st ed. 2020, pp. 607–617). Springer. https://doi.org/10.1007/978-981-15-5436-0_47

Mariotti, A., Blard, P. H., Charreau, J., Petit, C., & Molliex, S. (2019). Denudation systematics inferred from in situ cosmogenic 10Be concentrations in fine (50–100 µm) and medium (100–250 µm) sediments of the Var River basin, southern French Alps. Earth Surface Dynamics, 7(4), 1059–1074. https://doi.org/10.5194/esurf-7-1059-2019

Mas, V. (2009). Caractérisation de l'activité hydrosédimentaire dans le système turbiditique du Var (NO Méditerranée) et de son enregistrement dans l'archive sédimentaire [Sédimentologie Marine et Paléoclimats]. Université Bordeaux I, Bordeaux.

Migeon, S. (2006). MALISAR. French Oceanographic Cruises. https://doi.org/10.18142/207

Migeon, S., Savoye, B., & Faugeres, J. C. (2000). Quaternary development of migrating sediment waves in the Var deep-sea fan: distribution, growth pattern, and implication for levee evolution. Sedimentary Geology, 133(3-4), 265–293. https://doi.org/10.1016/S0037-0738(00)00043-9

Migeon, S., Savoye, B., Zanella, E., Mulder, T., Faugères, J.-C., & Weber, O. (2001). Detailed seismic-reflection and sedimentary study of turbidite sediment waves on the Var Sedimentary Ridge (SE France): significance for sediment transport and deposition and for the mechanisms of sediment-wave construction. Marine and Petroleum Geology, 18(2), 179–208. https://doi.org/10.1016/S0264-8172(00)00060-X

Migeon, S., Cattaneo, A., Hassoun, V., Larroque, C., Corradi, N., Fanucci, F., Dano, A., Mercier de Lepinay, B., Sage, F., & Gorini, C. (2011). Morphology, distribution and origin of recent submarine landslides of the Ligurian Margin (North-western Mediterranean): some insights into geohazard assessment. Marine Geophysical Research, 32, 225–243). https://doi.org/10.1007/s11001-011-9123-3

Mulder, T., Migeon, S., Savoye, B., & Jouanneau, J. M. (2001). Twentieth century floods recorded in the deep Mediterranean sediments. Geology, 29(11), 1011. https://doi.org/10.1130/0091-7613(2001)029%3C1011:TCFRIT%3E2.0.CO;2

Mulder, T., Savoye, B., Piper, D. J. W., & Syvitski, J. P. M. (1998). The Var submarine sedimentary system: understanding Holocene sediment delivery processes and their importance to the geological record. Geological Society, London, Special Publications, 129(1), 145–166. https://doi.org/10.1144/GSL.SP.1998.129.01.10

Mulder, T., Tisot, J. P., Cochonat, P., & Bourillet, J. F. (1994). Regional assessment of mass failure events in the Baie des Anges, Mediterranean Sea. Marine Geology, 122(1-2), 29–45. https://doi.org/10.1016/0025-3227(94)90203-8

Nash, J. E., & Sutcliffe, J. V. (1970). River flow forecasting through conceptual models part I — A discussion of principles. Journal of Hydrology. 10(3), 282–290. https://doi.org/10.1016/0022-1694(70)90255-6

Nasr-Azadani, M. M., & Meiburg, E. (2014). Turbidity currents interacting with three-dimensional seafloor topography. Journal of Fluid Mechanics, 745, 409–443. https://doi.org/10.1017/jfm.2014.47

Oliveros, C. (1996). Transports solids: modèles et conditions d'application en région PACA (Rapport BRGM R39474). Bureau de Recherches Géologiques et Minières.

Parker, G., Fukushima, Y., & Pantin, H. M. (1986). Self-accelerating turbidity currents. Journal of Fluid Mechanics, 171(1), 145. https://doi.org/10.1017/S0022112086001404

Parsons, J. D., Bush, J. W. M., & Syvitski, J. P. M. (2001). Hyperpycnal plume formation from riverine outflows with small sediment concentrations. Sedimentology, 48(2), 465–478. https://doi.org/10.1046/j.1365-3091.2001.00384.x

Piper, D. J. W., & Savoye, B. (1993). Processes of late Quaternary turbidity current flow and deposition on the Var deep-sea fan, north-west Mediterranean Sea. Sedimentology, 40(3), 557–582. https://doi.org/10.1111/j.1365-3091.1993.tb01350.x

Poggio, L., Sousa, L. M. de, Batjes, N. H., Heuvelink, G. B. M., Kempen, B., Ribeiro, E., & Rossiter, D. (2021). SoilGrids 2.0: producing soil information for the globe with quantified spatial uncertainty. SOIL, 7(1), 217–240. https://doi.org/10.5194/soil-7-217-2021

Postma, G., Nemec, W., & Kleinspehn, K. L. (1988). Large floating clasts in turbidites: a mechanism for their emplacement. Sedimentary Geology, 58(1), 47–61. https://doi.org/10.1016/0037-0738(88)90005-X

Salles, T., Lopez, S., Cacas, M. C., & Mulder, T. (2007). Cellular automata model of density currents. Geomorphology, 88(1-2), 1–20. https://doi.org/10.1016/j.geomorph.2006.10.016

Schoorl, J. M., Veldkamp, A., & Bouma, J. (2002). Modeling Water and Soil Redistribution in a Dynamic Landscape Context. Soil Science Society of America Journal, 66(5), 1610–1619. https://doi.org/10.2136/sssaj2002.1610

Skinner, C. J., Coulthard, T. J., Schwanghart, W., van de Wiel, M. J., & Hancock, G. (2018). Global sensitivity analysis of parameter uncertainty in landscape evolution models. Geoscientific Model Development, 11(12), 4873–4888. https://doi.org/10.5194/gmd-11-4873-2018

Talling, P. J., Cartigny, M. J. B., Pope, E., Baker, M., Clare, M. A., Heijnen, M., Hage, S., Parsons, D. R., Simmons, S. M., Paull, C. K., Gwiazda, R., Lintern, G., Hughes Clarke, J. E., Xu, J., Silva Jacinto, R., & Maier, K. L. (2023). Detailed monitoring reveals the nature of submarine turbidity currents. Nature Reviews Earth & Environment, 4(9), 642–658. https://doi.org/10.1038/s43017-023-00458-1

Teles, V., Chauveau, B., Joseph, P., Weill, P., & Maktouf, F. (2016). CATS – A process-based model for turbulent turbidite systems at the reservoir scale. Comptes Rendus Geoscience, 348(7), 489–498. https://doi.org/10.1016/j.crte.2016.03.002

van de Wiel, M. J., Coulthard, T. J., Macklin, M. G., & Lewin, J. (2007). Embedding reach-scale fluvial dynamics within the CAESAR cellular automaton landscape evolution model. Geomorphology, 90(3-4), 283–301. https://doi.org/10.1016/j.geomorph.2006.10.024

Virtanen, P., Gommers, R., Oliphant, T. E., Haberland, M., Reddy, T., Cournapeau, D., Burovski, E., Peterson, P., Weckesser, W., Bright, J., van der Walt, S. J., Brett, M., Wilson, J., Millman, K. J., Mayorov, N., Nelson, A. R. J., Jones, E., Kern, R., Larson, E., Carey, C. J., Polat, I., Feng, Y., Moore, E. W., VanderPlas, J., Laxalde, J., Perktold, J., Cimrmanm, R., Henriksen, I., Quintero, E. A., Harris, C. R., Archibald, A. M., Ribeiro, A. H., Pedregosa, F., & van Mulbregt, P. (2020). Scipy 1.0: Fundamental algorithms for scientific computing in Python.

Nature Methods, 17(3), 261–272. https://doi.org/10.1038/s41592-019-0686-2

Yassine, R., Lastes, M., Argence, A., Gandouin, A., Imperatrice, C., Michel, P., Zhang, R., Brigode, P., Delestre, O., & Taccone, F. (2020). Simulation of the Alex Storm Flash-Flood in the Vésubie Catchment (South Eastern France) Using Telemac-2D Hydraulic Code. In P. Gourbesville & G. Caignaert (Eds.), Springer Water. Advances in Hydroinformatics: SimHydro 2019 - Models for Extreme Situations and Crisis Management (1st ed. 2020, pp. 847–863). Springer. https://doi.org/10.1007/978-981-19-1600-7_52

How to cite: Remaud, A., Armitage, J. J., Teles, V., Rohais, S., & Mulder, T. (2024). From flood to turbidity current: combined models to simulate continent to ocean sediment transport in the Var system, France. Sedimentologika, 2(2), 1-21. https://doi.org/10.57035/journals/sdk.2024.e22.1538